

# Green Synthesis of Silver and Titanium Dioxide Nanoparticles Using *Euphorbia prostrata* Extract Shows Shift from Apoptosis to G<sub>0</sub>/G<sub>1</sub> Arrest followed by Necrotic Cell Death in *Leishmania donovani*

Abdul Abdus Zahir,<sup>a</sup> Indira Singh Chauhan,<sup>b</sup> Asokan Bagavan,<sup>a</sup> Chinnaperumal Kamaraj,<sup>a</sup> Gandhi Elango,<sup>a</sup> Jai Shankar,<sup>d</sup> Nidhi Arjaria,<sup>d</sup> Selvaraj Mohana Roopan,<sup>c</sup> Abdul Abdul Rahuman,<sup>a</sup> Neeloo Singh<sup>b</sup>

Unit of Nanotechnology and Bioactive Natural Products, Post Graduate and Research Department of Zoology, C. Abdul Hakeem College, Melvisharam, Vellore District, Tamil Nadu, India<sup>a</sup>; Biochemistry Division, CSIR Central Drug Research Institute, Jankipuram Extension, Lucknow, India<sup>b</sup>; Organic & Medicinal Chemistry Research Laboratory, Organic Chemistry Division, School of Advanced Sciences, VIT University, Vellore, Tamil Nadu, India<sup>c</sup>; Transmission Electron Microscopy, CSIR Indian Institute of Toxicology Research, Lucknow, India<sup>d</sup>

The aim of the present study was to synthesize silver (Ag) and titanium dioxide (TiO<sub>2</sub>) nanoparticles (NPs) using green synthesis from aqueous leaf extract of *Euphorbia prostrata* as antileishmanial agents and to explore the underlying molecular mechanism of induced cell death. *In vitro* antileishmanial activity of synthesized NPs was tested against promastigotes of *Leishmania donovani* by alamarBlue and propidium iodide uptake assays. Antileishmanial activity of synthesized NPs on intracellular amastigotes was assessed by Giemsa staining. The leishmanicidal effect of synthesized Ag NPs was further confirmed by DNA fragmentation assay and by cell cycle progression and transmission electron microscopy (TEM) of the treated parasites. TEM analysis of the synthesized Ag NPs showed a spherical shape with an average size of 12.82 ± 2.50 nm, and in comparison to synthesized TiO<sub>2</sub> NPs, synthesized Ag NPs were found to be most active against *Leishmania* parasites after 24 h exposure, with 50% inhibitory concentrations (IC<sub>50</sub>) of 14.94 µg/ml and 3.89 µg/ml in promastigotes and intracellular amastigotes, respectively. A significant increase in G<sub>0</sub>/G<sub>1</sub> phase of the cell cycle with a subsequent decrease in S (synthesis) and G<sub>2</sub>/M phases compared to controls was observed. The growth-inhibitory effect of synthesized Ag NPs was attributed to increased length of S phase. A decreased reactive oxygen species level was also observed, which could be responsible for the caspase-independent shift from apoptosis (G<sub>0</sub>/G<sub>1</sub> arrest) to massive necrosis. High-molecular-weight DNA fragmentation as a positive consequence of necrotic cell death was also visualized. We also report that the unique trypanothione/trypanothione reductase (TR) system of *Leishmania* cells was significantly inhibited by synthesized Ag NPs. The green-synthesized Ag NPs may provide promising leads for the development of cost-effective and safer alternative treatment against visceral leishmaniasis.

Neglected diseases caused by parasites are the second leading cause of mortality, and they impose a substantial burden of morbidity around the globe and more predominantly in developing countries. Leishmaniasis currently threatens 350 million people in 88 countries around the world. Two million new cases are thought to occur annually, with an estimated 12 million people presently infected (1). Among different leishmanial infections, visceral leishmaniasis (VL) caused by *Leishmania donovani* is the most threatening. Although miltefosine and amphotericin B are used for clinical treatment, the antileishmanial drug arsenal still requires improvement (2). For instance, miltefosine monotherapy has failed to cure relapsing VL in HIV-infected patients, and thus its role against HIV-associated VL remains unclear (3).

Nanomedicine is defining the use of nanotechnology in medicine, which has been of great interest in recent years. The use of nanoparticles (NPs) for therapeutics is one of the purposes of nanomedicine (4, 5). In recent years, an increasing percentage of nanomaterials have emerged and made advancement in different fields. NPs play an indispensable role in drug delivery, diagnostics, imaging, sensing, gene delivery, artificial implants, and tissue engineering (6). Sinha et al. (7) have reported that the biosynthesis of NPs is advantageous over chemical and physical methods, as it is a cost-effective and environment-friendly method, where it is not necessary to use high pressure, high energy, high temperatures, or toxic chemicals. Silver nanoparticles (Ag NPs) have several important applications in the field of biolabeling, sensors, antimicrobial

agents, and filters. They are capable of purifying drinking water, degrading pesticides, and killing human-pathogenic bacteria (8). Ag NPs have been used in the treatment and improvement of drug delivery against leishmaniasis (9–12). Silver polypyridyl complexes are biologically active against *Leishmania mexicana*, where they interact with DNA (13). Similarly, nanopreparations with titanium dioxide nanoparticles (TiO<sub>2</sub> NPs) are under investigation as novel treatments for acne vulgaris, recurrent condyloma acuminatum, atopic dermatitis, hyperpigmented skin lesions, and other nondermatologic diseases (14). Quercetin (polyphenolic

Received 20 January 2015 Returned for modification 16 February 2015

Accepted 18 May 2015

Accepted manuscript posted online 1 June 2015

Citation Zahir AA, Chauhan IS, Bagavan A, Kamaraj C, Elango G, Shankar J, Arjaria N, Roopan SM, Rahuman AA, Singh N. 2015. Green synthesis of silver and titanium dioxide nanoparticles using *Euphorbia prostrata* extract shows shift from apoptosis to G<sub>0</sub>/G<sub>1</sub> arrest followed by necrotic cell death in *Leishmania donovani*. Antimicrob Agents Chemother 59:4782–4799. doi:10.1128/AAC.00098-15.

Address correspondence to Abdul Abdul Rahuman, abdulrahuman6@hotmail.com, or Neeloo Singh, neeloo888@yahoo.com.

A.A.Z. and I.S.C. contributed equally to this work.

This is CDRI communication no. 8767.

Copyright © 2015, American Society for Microbiology. All Rights Reserved.

doi:10.1128/AAC.00098-15

compound)-conjugated gold NPs have also been evaluated against promastigotes and amastigotes of *L. donovani* (15).

There are limited studies concerning the green synthesis of NPs and its efficacy in controlling *Leishmania* parasites. Among the various biosynthetic approaches, the use of plant extracts is preferable, as they are readily available and safe to handle and possess a broad viability of metabolites. The potential of plants as biological materials for the synthesis of NPs is yet to be fully explored (16). *Euphorbia prostrata* is a small, prostrate, hispidly pubescent annual herb found all over India. Leaf extracts of *E. prostrata* exhibit antibacterial, nematicidal, and antiparasitic activities (17). Anthraquinones, flavonoids, phenols, phlobatannins, polysaccharides, saponins, tannins, and terpenoids have been isolated from the leaf extract of *E. prostrata* (18). The flavonoids are promising compounds for controlling human and animal parasitic diseases (19). Phenolic compounds were tested against *Leishmania* spp. and for immunomodulatory effects on macrophages (20). Similarly, the antileishmanial activities of terpenoid derivatives were tested against promastigotes and intracellular amastigotes form of *L. donovani* (21). In the present study, the antileishmanial activities of Ag NPs and TiO<sub>2</sub> NPs that were green synthesized using the aqueous leaf extract of *E. prostrata* were evaluated against promastigotes and intracellular amastigotes of *L. donovani*.

## MATERIALS AND METHODS

**Synthesis of Ag NPs and TiO<sub>2</sub> NPs.** Fresh leaves of *E. prostrata* were collected in and around Melvisharam, Vellore District, Tamil Nadu, India. The aqueous leaf extract was prepared by placing 2 g of finely cut leaves in a 250-ml Erlenmeyer flask along with 100 ml of sterilized double-distilled water and boiling the mixture at 60°C for 15 to 20 min. The extract was filtered with Whatman filter paper no. 1, stored at -20°C, and used within a week. The biosynthesis of Ag NPs was carried out using different compositions of the aqueous leaf extract with AgNO<sub>3</sub> solution (3:97, 6:94, 9:91, 12:88, and 15:85 ml). The reaction mixture was periodically observed for the change in color and analyzed by a UV-visible spectrum (UV-Vis) spectrophotometer in the range of 100 to 700 nm. A total volume of 88 ml of 1 mM AgNO<sub>3</sub> solution was reduced using 12 ml of aqueous leaf extract of *E. prostrata* at room temperature for 6 h, resulting in a brown-yellow solution, indicating the formation of synthesized Ag NPs (22). For synthesis of TiO<sub>2</sub> NPs, the Erlenmeyer flask containing 100 ml of 5 mM TiO(OH)<sub>2</sub> was stirred for 2 h. Different proportions of aqueous leaf extract of *E. prostrata* were prepared and interacted with the TiO(OH)<sub>2</sub> solution at mixing ratios of 5:95, 10:90, 15:85, 20:80, and 25:75 ml, separately. Aqueous leaf extract (20 ml) from *E. prostrata* was added to 80 ml of TiO(OH)<sub>2</sub> solution for the optimization of TiO<sub>2</sub> NP synthesis. The pure TiO(OH)<sub>2</sub> solution and the aqueous leaf extract did not show any color change, whereas the leaf extract with TiO(OH)<sub>2</sub> showed a color change to light green. Different reaction parameters (concentrations of plant extract, substrate concentrations, pH, temperature, and reaction time) were optimized to synthesize NPs with controlled properties (23).

**Characterization of synthesized NPs.** Synthesis of NPs solution with leaf extract was observed by UV-Vis spectroscopy. The bioreduction of ions in the solutions was monitored by periodic sampling of aliquots (1 ml) of the aqueous component after 20× dilution and measured in the UV-Vis spectra. Samples were monitored as a function of time of reaction using Shimadzu 1601 spectrophotometer in the 100- to 700-nm range operated at a resolution of 1 nm. The reduced solution was centrifuged at 8,000 rpm for 40 min, and the resulting pellet was redispersed in deionized water. Adsorbed substances on the surfaces of the synthesized NPs were removed by repeated washing.

The purified and dried pellets of synthesized Ag NPs and TiO<sub>2</sub> NPs were subjected to X-ray diffraction (XRD) analysis. For XRD studies,

dried NPs were used to coat XRD grids, and the spectra were recorded by using a Phillips PW 1830 instrument operating at a voltage of 40 kV and a current of 30 mA with Cu Kα1 radiation. Fourier transform infrared (FTIR) analysis of the samples was carried out using a PerkinElmer spectrophotometer in the diffuse reflectance mode at a resolution of 4 cm<sup>-1</sup> in KBr pellets and showed possible functional groups for the formation of NPs. Topography of synthesized NPs was studied using atomic force microscopy (AFM) analysis (Innova microscope; Veeco, USA). Images were processed using XEI software (Park Systems). The synthesized NPs were examined using an Innova advanced scanning probe microscope (CP-II; Veeco Instruments Inc., USA) in a noncontact tapping mode. A thin film of the sample was prepared on a glass slide by dropping 100 μl of the sample on the slide and allowed to dry for 5 min. Topographical images were obtained in noncontact mode using silicon nitride tips at a resonance frequency of 218 kHz in ambient air by oscillating the cantilever assembly at or near the cantilever's resonant frequency using a piezoelectric crystal. Characterization was done by observing the patterns of surface topography, and data analysis was done with WSXM software (24). The size of the NPs was confirmed by using transmission electron microscopy (TEM) analysis (Hitachi H-7100 electron microscope) using an accelerating voltage of 120 kV and methanol as the solvent.

**GC-MS analysis.** The chemical composition of aqueous leaf extract of *E. prostrata* was analyzed by using gas chromatography-mass spectrometry (GC-MS) (GCD-HP1800A system; Hewlett-Packard, USA) on a system equipped with a split/splitless capillary injection port. For GC-MS detection, an electron ionization system (quadrupole analyzer; mass range, 10 to 425 atomic mass units [amu]) with an ionization energy of 70 eV was used. Each of these steps was carried out under high vacuum from 10<sup>-4</sup> to 10<sup>-8</sup> torr. Helium gas was used as a carrier at a constant flow rate of 1 ml/min. Injector and mass transfer line temperatures were set at 250°C and 280°C, respectively. The components of aqueous leaf extract of *E. prostrata* were identified after comparison with the available data in the NIST library attached to the GC-MS instrument and reported (25).

**Macrophage culture.** The J774A.1 mouse (BALB/c) macrophage cell line was obtained from the National Centre for Cell Science (Pune, India) and used as a cellular host for the *in vitro* intracellular test of antileishmanial activity against amastigotes. The cells were maintained in RPMI 1640 medium (Gibco-BRL) adjusted to contain 2 g of sodium bicarbonate/liter, 6 g of HEPES/liter, 10% (vol/vol) heat-inactivated fetal bovine serum (HI-FBS; Gibco, Germany), and 100 U penicillin and 100 μg of streptomycin/ml at 37°C in a humidified atmosphere of 95% air and 5% CO<sub>2</sub> (26).

**Parasite culture and analysis of cell viability.** Promastigotes of *L. donovani* (strain MHOM/IN/80/DD8) were routinely cultured as described previously (27). The cell viability reagent alamarBlue (catalog no. DAL1025; Invitrogen, Carlsbad, CA) was used for evaluation of antileishmanial activity of synthesized Ag NPs. Logarithmic-phase promastigotes of *L. donovani* (50,000 cells; final volume, 200 μl/well) were seeded in 96-well microtiter plates (Greiner Bio-One, Germany) in the presence of different concentrations (0, 12.5, 25, 50, and 100 μg/ml) of synthesized Ag NPs and incubated at 25°C for 24 h. Miltefosine was used as the standard drug. alamarBlue (20 μl) was added to each well and the plate was further incubated at 25°C for 4 h. Absorbance was measured in an enzyme-linked immunosorbent assay (ELISA) reader (Biotek Instruments, Epoch) using 570 nm as the test wavelength (resorufin) and 600 nm as the reference wavelength (resazurin), serving as a blank. The oxidized form of alamarBlue resazurin (nontoxic, cell permeant, and blue) was reduced by metabolically active cells to resorufin (highly fluorescent and red). The percent cell viability of promastigotes treated with synthesized Ag NPs was analyzed by the following formula (28): [untreated control λ (570 - 600 nm) - treated set λ (570 - 600 nm)]/untreated control λ (570 - 600 nm) × 100.

***In vitro* evaluation of antileishmanial activity of synthesized Ag NPs in intracellular amastigotes.** J774A.1 mouse (BALB/c) macrophages, 4,000 cells per well, in a final volume of 200 μl of RPMI 1640 medium were seeded in 8-well chamber slides (Nunc Lab-Tek II chamber slide system).

The cells were allowed to adhere for 8 h at 37°C in a carbon dioxide incubator with 5% CO<sub>2</sub>. Nonadherent cells were removed, and these cells were infected with stationary-phase promastigotes of *L. donovani* at a ratio of 6:1 (parasites/macrophages) and incubated at 37°C in 5% CO<sub>2</sub> for 0 to 18 h. At 18 h after the parasites entered macrophages, free parasites were eliminated, and infected macrophages were treated with increasing concentrations (0, 2.5, 5, and 10 µg/ml) of synthesized Ag NPs and incubated at 37°C in 5% CO<sub>2</sub> for 24 h. After incubation for various times, infected macrophages treated with or without synthesized Ag NPs in chamber slides were fixed with ice-cold methanol, and slides were then submerged in 10% (vol/vol) Giemsa staining solution (Thomas Baker) for 45 min, briefly washed in water, and set to dry. The slides were viewed on an inverted bright-field microscope (IX73 inverted microscope; Olympus) (29). At least 100 macrophages per well from duplicate cultures were counted to calculate the percentage of infected macrophages using the following formula (30): % reduction = number of amastigotes per 100 macrophages (treated samples)/number of amastigotes per 100 macrophages (infected control) × 100.

IC<sub>50</sub>, the concentration of drug that is cytotoxic to 50% of the amastigotes, was obtained by plotting the graph of percentage of cell viability versus different concentrations of synthesized Ag NPs.

**In vitro cytotoxicity in macrophages.** The J774A.1 cells were incubated in a 96-well plate containing 50,000 cells/well. The plates were incubated overnight in a CO<sub>2</sub> incubator, with a supply of 5% CO<sub>2</sub> at 37°C. The synthesized Ag NPs, at different concentrations (0, 5, 10, and 20 µg/ml) was dispensed in triplicate, and three wells were left as control wells. The plates were incubated for 24 h, and an MTT [3-(4,5-dimethylthiazole-2-yl)-2,5-diphenyl tetrazolium bromide] assay was performed to assess cell proliferation or viability (27). The 50% cytotoxic concentration (CC<sub>50</sub>) was determined by logarithmic regression analysis using GraphPad Prism 5 software.

**Transmission electron microscopy.** TEM analysis was carried out to observe the ultrastructural changes in the morphology of *L. donovani* promastigotes induced by synthesized Ag NPs. Parasites were incubated in the presence of synthesized Ag NPs at the IC<sub>50</sub> for 45 min and washed with phosphate-buffered saline (PBS) (pH 7.2) prior to fixing in 2.5% glutaraldehyde in sodium cacodylate (Ladd Research Industries, USA) buffer (pH 7.2) for 2 h at 4°C. Fixed parasites were centrifuged at 3,500 × g for 10 min, washed 3 times with 0.1 M sodium cacodylate buffer, and postfixed in 1% osmium tetroxide for 2 h. Postfixed parasites were washed with sodium cacodylate, dehydrated in an ascending acetone series (15, 30, 60, and 100%), embedded in an araldite-dodecyl succinic anhydride mixture (Ladd Research Industries, USA), and baked at 60°C for 48 h. After baking, blocks were cut (60 to 80 nm thick) with an ultramicrotome (Leica EM UC7, Vienna, Austria), mounted on copper grids, and double stained with uranyl acetate and lead citrate. Stained sections were examined by TEM (Tecnai G2 Spirit; FEI, Netherlands) equipped with a Gatan Orius camera at 80 kV (31).

**Propidium iodide uptake assay.** Logarithmic-phase promastigotes of *L. donovani* (1 × 10<sup>6</sup> cells; final volume, 2 ml/well) were seeded in 6-well microtiter plates (Greiner Bio-One, Germany) in the presence of different concentrations (12.5, 25, and 50 µg/ml) of synthesized Ag NPs and incubated at 25°C for 24 h. After various incubation times, cells were centrifuged (3,500 × g for 10 min), washed once with PBS (pH 7.2), resuspended in a 50-µg/ml final concentration of propidium iodide (PI) (catalog no. SLBF5585V; Sigma-Aldrich, St. Louis, MO, USA), and incubated for 30 min in the dark at room temperature. Unbound PI was removed by washing, and samples were processed on a FACSCalibur flow cytometer (BD Bioscience, San Jose, CA, USA). Fluorescence of the PI was collected in the FL2 channel, equipped with a 585/42-nm band pass filter. Analysis for mean fluorescence intensity was done using CellQuest Pro software (BD Biosciences, CA). A total of 20,000 events from each sample were acquired to ensure adequate data, and the histograms and images are representative of three independent experiments (32, 33).

**Analysis of externalized phosphatidylserine.** To quantify the percentage of parasites undergoing apoptosis, dual staining with annexin V–fluorescein isothiocyanate (FITC) and PI was performed as per the manufacturer's instructions (annexin V-FITC apoptosis detection kit; Sigma, MO, USA). In brief, log-phase *L. donovani* promastigotes (2 × 10<sup>6</sup> cells/ml) were treated with different concentrations (12.5, 25, and 50 µg/ml) of synthesized Ag NPs for 24 h, and cells were centrifuged (3,500 × g for 5 min), washed twice in PBS, and resuspended in annexin V binding buffer (10 mM HEPES/NaOH [pH 7.4], 140 mM NaCl, and 2.5 mM CaCl<sub>2</sub>). Annexin V-FITC and PI were then added according to the manufacturer's instructions and incubated for 15 min in the dark at 20 to 25°C. The percentages of viable and dead cells were determined from 10,000 cells per sample by using the FL1 channel for annexin V and the FL2 channel for PI on a FACSCalibur flow cytometer (BD Bioscience, San Jose, CA, USA). The histogram and images are representative of three independent experiments (34).

**Cell cycle analysis.** Briefly, log-phase *L. donovani* promastigotes (2 × 10<sup>6</sup> cells/ml) were treated with different concentrations (12.5, 25, and 50 µg/ml) of synthesized Ag NPs for 24 h and were harvested by centrifugation at 3,500 × g for 5 min at 4°C. Cells were washed once in 1 ml PBS and then fixed by incubation in 70% ethanol–30% PBS for 1 h at 4°C. Fixed cells were harvested by centrifugation at 1750 × g for 10 min at 4°C, washed in 1 ml PBS, and resuspended in 1 ml PBS with RNase A (100 µg/ml; catalog no. EN0531; Fermentas) and PI (10 µg/ml). The cells were incubated at room temperature for 45 min and then analyzed using a FACSCalibur flow cytometer (BD Bioscience, San Jose, CA, USA). Cell cycle distribution was modeled using ModFit LT for Mac V3.0, and 10,000 events from each sample were acquired to ensure adequate data (34). The histograms and images are representative of three independent experiments.

**DNA fragmentation assay.** Qualitative analysis of fragmentation was performed by agarose gel electrophoresis of total genomic DNA of treated and untreated parasites (34). Total cellular DNA from promastigotes exposed to different concentrations (12.5, 25, and 50 µg/ml) of synthesized Ag NPs was isolated with an apoptotic DNA ladder detection kit according to the manufacturer's instructions (catalog no. KHO1021; Molecular Probes, USA). The isolated DNA was quantified spectrophotometrically at an absorbance ratio of 260/280 nm, and DNA (1 µg/lane) was separated on 1.2% agarose gels containing ethidium bromide in TBE buffer (50 mM; pH 8.0) for 1.5 h at 75 V, visualized under UV light, and photographed using a gel documentation system (Genei, Uvitec Cambridge).

**TUNEL assay.** Fragmentation of DNA into nucleosomal bands, as a function of apoptotic cell death, was studied with a DNA laddering assay. DNA fragmentation within the cell can be analyzed by terminal deoxynucleotidyltransferase (TdT)-mediated dUTP nick end labeling (TUNEL) using an APO-BRDU assay kit (a flow cytometry kit for apoptosis; Sigma) according to the manufacturer's instructions. The TUNEL technique is able to quantify the proportion of DNA fragments by binding to BrdU via TdT. Thus, the amount of DNA fragments is directly proportional to the fluorescence obtained by BrdU incorporation and labeling by anti-BrdU antibody conjugated to FITC. Briefly, promastigotes were incubated with different concentrations (12.5, 25, and 50 µg/ml) of synthesized Ag NPs for 24 h, washed twice in PBS (pH 7.2), and fixed in 1% paraformaldehyde for 15 min. The cells were washed again in PBS and incubated in ice-cold 70% (vol/vol) ethanol for 30 min in a –20°C freezer. After centrifugation, the cells were allowed to react with TdT in DNA-labeling solution for 60 min at 37°C. The samples were incubated with an antibody-staining solution containing the FITC-labeled anti-BrdU antibody. Finally, the cells were counterstained with propidium iodide, and fluorescence acquired with a FACSCalibur flow cytometer (BD Bioscience, San Jose, CA, USA) through a dual-pass FITC/PI filter set. Two dual-parameter and two single-parameter displays were created with the flow cytometer data acquisition software (CellQuest Pro software; BD Biosciences, CA). The gating display was the standard dual-parameter DNA doublet discrimination display, with the DNA area signal on the



*y* axis and the DNA width on the *x* axis. From this display, a gate was drawn around the nonclumped cells, and the second gated dual-parameter display was generated. The DNA (linear red fluorescence) was displayed on the *x* axis, and anti-BrdU-FITC (log green fluorescence) was on the *y* axis. Two single-parameter gated histograms, DNA and FITC-BrdU, were also added to determine apoptotic cells and their cell cycle stages. The histogram and images are representative of three independent experiments. A total of 10,000 events from each sample were acquired to ensure adequate data (35).

**Measurement of ROS levels.** Intracellular reactive oxygen species (ROS) levels were measured in *L. donovani* promastigotes as described previously (36). Briefly, log-phase *L. donovani* promastigotes ( $2 \times 10^6$  cells/ml) treated with different concentrations of synthesized Ag NPs (12.5, 25, and 50  $\mu\text{g/ml}$ ) for 24 h, were washed and resuspended in 500  $\mu\text{l}$  of M-199 medium and loaded with the cell-permeant probe 2,7-dichlorodihydrofluorescein diacetate ( $\text{H}_2\text{DCFDA}$ ; 10  $\mu\text{M}$ ; Sigma) for 30 min at 20 to 25°C, and fluorescence was monitored. Use of the fluorescent probe  $\text{H}_2\text{DCFDA}$  is one of the most widely used techniques for direct measuring of the redox state of a cell. It is a cell-permeant and relatively nonfluorescent molecule. It is also extremely sensitive to the changes in the redox state of a cell and can be used to follow the changes of ROS over time. The activity of cellular esterases cleaves  $\text{H}_2\text{DCFDA}$  into 2,7-dichlorodihydrofluorescein ( $\text{DCFH}_2$ ). Peroxidases, cytochrome *c*, and  $\text{Fe}^{2+}$  can all oxidize  $\text{DCFH}_2$  to 2,7-dichlorofluorescein (DCF) in the presence of hydrogen peroxide. Accumulation of DCF in the cells was measured by an increase in fluorescence at 530 nm when the sample was excited at 485 nm. This increase is assumed to be proportional to the concentration of hydrogen peroxide in the cells (34). Fluorescence of 2,7-dichlorofluorescein (DCF) was collected in the FL1 channel on a FACSCalibur flow cytometer equipped with a 530/30-nm band pass filter (BD Bioscience). Fluorescence was measured in the log mode using CellQuest Pro software (BD Biosciences, CA) and expressed as mean fluorescence intensity. A total of 10,000 events from each sample were acquired to ensure adequate data. The histograms and images are representative of three independent experiments.

**Measurement of intracellular nonprotein thiols.** 5-Chloromethylfluorescein-diacetate (CMFH-DA; CellTracker green CMFDA, catalog no. C7025; Molecular Probes, USA) is a cell-permeant, nonfluorescent dye that, upon entering the cell, rapidly binds nonprotein thiols and becomes nonpermeant; the simultaneous cleavage of the diacetate moiety by cellular esterases yields a fluorescent thioether. Accordingly, the detected fluorescence is directly proportional to the amount of intracellular nonprotein thiols (37). Log-phase *L. donovani* promastigotes ( $2 \times 10^6$  cells/ml) treated with aqueous leaf extract of *E. prostrata*, synthesized Ag NPs, and  $\text{AgNO}_3$  solution for 24 h were collected in 1.5-ml microcentrifuge tubes and centrifuged at  $1,000 \times g$  for 5 min to remove the supernatant. Then, the cell pellets were washed with PBS, incubated with 5-chloromethylfluorescein-diacetate in the dark for 15 min at 37°C, and analyzed for fluorescence in the FL1 channel on a FACSCalibur flow cytometer equipped with a 530/30-nm band pass filter (BD Bioscience), and mean fluorescence intensity was determined by using CellQuest Pro software. A total of 40,000 events from each sample were acquired to ensure adequate data. The histogram and images are representative of three independent experiments.

**Statistical analysis.** Each experiment was performed at least three times. The data presented are means  $\pm$  standard deviations (SD). The comparison of groups was done by one-way analysis of variance (ANOVA) using GraphPad Prism software. The groups were compared by Dunnett's test after one-way ANOVA. Individual comparisons were done with the Newman-Keuls test. A *P* value of 0.05 is considered the level of significance.

## RESULTS

The leaf extract of *E. prostrata* was mixed in the aqueous solution of the silver ion complex, and it started to change color from

watery to brown due to reduction of silver ion, which indicated the formation of Ag NPs. NP formation was monitored by color change, since color change has been reported to be the initial evidence of NP formation (23). Results of the present study revealed that the overall optimized reaction conditions for the synthesis of Ag NPs were as follows: concentration of aqueous leaf extract, 12 ml; concentration of  $\text{AgNO}_3$  solution, 88 ml of 1 mM; temperature, 45°C; pH, 9.0; time, 6 h; maximum absorption peaks observed at 420 nm. Similarly, optimized reaction conditions for synthesized  $\text{TiO}_2$  NPs were: concentration of aqueous leaf extract, 20 ml; concentration of  $\text{TiO}(\text{OH})_2$  solution, 80 ml of 5 mM; temperature, 40°C; pH, 8.0; time, 10 h; maximum absorption peak observed at 305 nm. These results are in good agreement with previous reports (23).

**Characterization of synthesized NPs.** The synthesis of Ag NPs using *E. prostrata* leaf extract was supported by X-ray diffraction measurements. The XRD spectrum was compared with the standard confirmed spectrum of Ag particles formed in the present experiments, which were in the form of nanocrystals, as evidenced by the peaks at  $2\theta$  values of 38.26°, 44.45°, 64.58°, and 77.49°, which were indexed to the planes 111, 200, 220, and 311, respectively. The average grain size of Ag NPs formed in the biosynthesis was determined to be  $12.82 \pm 2.50$  nm for the higher-intensity peak using Scherrer's formula,  $d = 0.89\lambda/\beta \cos\theta$ . XRD analysis of the synthesized  $\text{TiO}_2$  NPs showed distinct diffraction peaks at 27.63°, 36.27°, 41.43°, 54.49°, 56.80°, and 69.16° indexed to the planes 110, 101, 111, 211, 220 and 301, respectively (Fig. 1A). The average grain size of  $\text{TiO}_2$  NPs formed in the biosynthesis was determined to be  $83.22 \pm 1.50$  nm. The sharp peaks and the absence of unidentified peaks confirmed the crystallinity and higher purity of prepared NPs. Dubey et al. (38) reported that the size of nanosilver as estimated from the full width at half maximum of the 111 peak of silver using the Scherrer's formula was 20 to 80 nm. XRD peaks at a  $2\theta$  value of 25.25° (plane 101) confirm the characteristic facets for the anatase form of  $\text{TiO}_2$  (39). This estimation confirmed the hypothesis of particle monocrystallinity. The sharpening of the peaks clearly indicates that the particles were in the nanoregime.

FTIR spectroscopy is used to probe the chemical composition of the surface and capping agents for the synthesis of NPs. FTIR analysis of synthesized Ag NPs and  $\text{TiO}_2$  NPs using the aqueous leaf extract of *E. prostrata* are shown in Fig. 1B. The synthesized Ag NPs showed the presence of bands due to heterocyclic amine, NH stretch ( $3,431 \text{ cm}^{-1}$ ), methylene C-H bend ( $1,616 \text{ cm}^{-1}$ ), gem-dimethyl ( $1,381 \text{ cm}^{-1}$ ), cyclohexane ring vibrations ( $1,045 \text{ cm}^{-1}$ ), skeletal C-C vibrations ( $818 \text{ cm}^{-1}$ ), and aliphatic iodo compounds with C-I stretch ( $509 \text{ cm}^{-1}$ ). The functional groups for *E. prostrata* leaf aqueous extract and synthesized Ag NPs were 548 and  $509 \text{ cm}^{-1}$  for aliphatic iodo compounds with C-I stretch. This proves that Ag NPs were synthesized with plant compounds involved in the biological reduction of  $\text{AgNO}_3$ . Similarly, the synthesized  $\text{TiO}_2$  NPs showed the presence of bands due to hydroxy groups, H-bonded OH stretch ( $3,420 \text{ cm}^{-1}$ ), methylene C-H asymmetrical/symmetrical stretch ( $2,926 \text{ cm}^{-1}$ ), secondary amine with NH bend ( $1,618 \text{ cm}^{-1}$ ), phenol or tertiary alcohol with OH bend ( $1,377 \text{ cm}^{-1}$ ), cyclic ethers of large rings with C-O stretch ( $1,071 \text{ cm}^{-1}$ ), and thioethers,  $\text{CH}_3\text{-S}$  with C-S stretch ( $649 \text{ cm}^{-1}$ ). The functional groups of leaf extract and synthesized  $\text{TiO}_2$  NPs were 2,924 and  $2,926 \text{ cm}^{-1}$  for methylene C-H asymmetrical/symmetrical stretch and 1,618 and  $1,618 \text{ cm}^{-1}$  for secondary

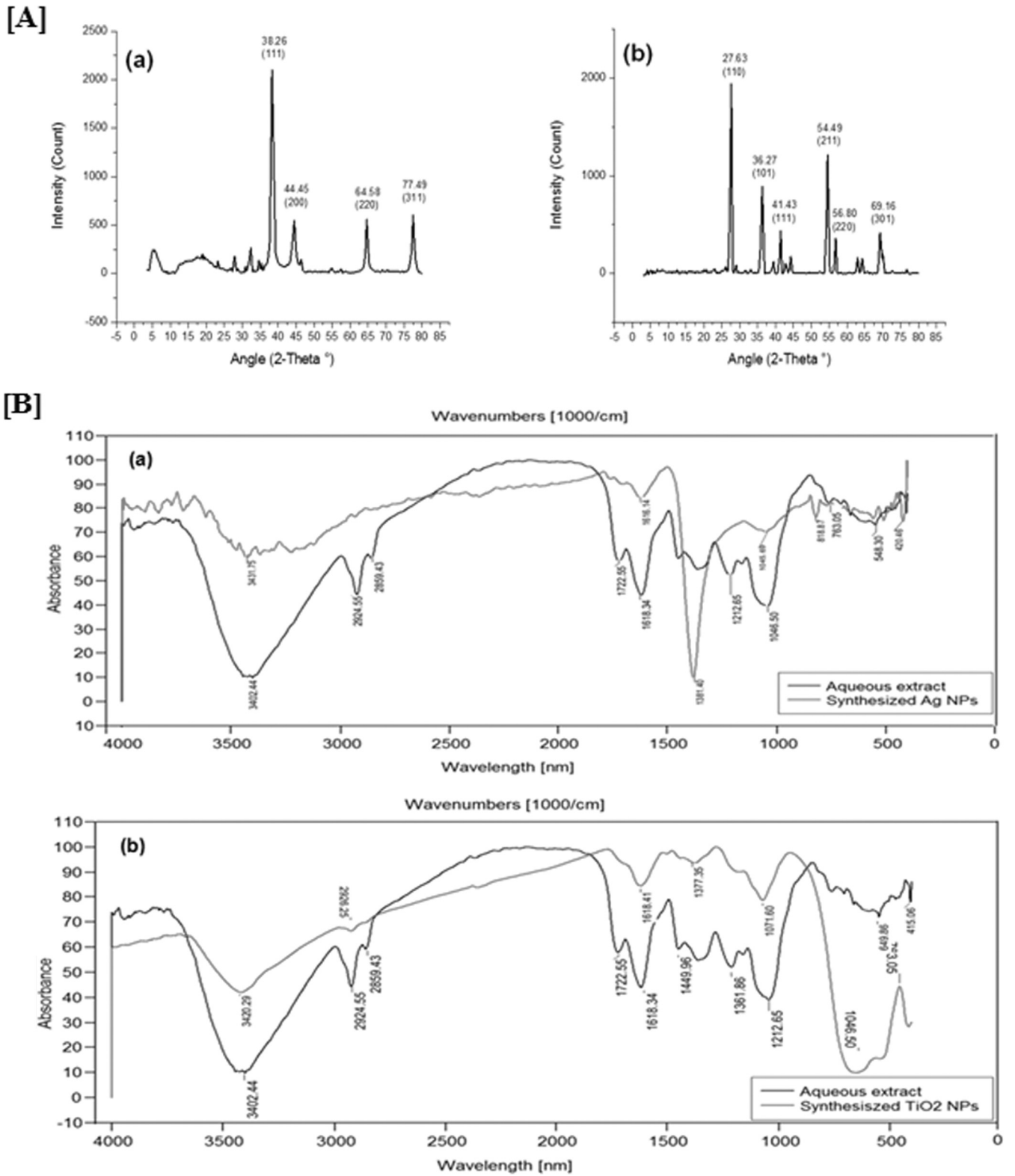


**FIG 1** (A) Characterization of synthesized (Ag and TiO<sub>2</sub>) NPs. The XRD patterns of Ag NPs (a) and TiO<sub>2</sub> NPs (b) synthesized by using *E. prostrata* are shown. (B) FTIR spectra of vacuum-dried powder of synthesized Ag NPs from *E. prostrata* (a) and of vacuum-dried powder of synthesized TiO<sub>2</sub> NPs from aqueous leaf extracts of *E. prostrata* (b).

amine with NH bend. After reduction of  $\text{TiO}(\text{OH})_2$ , the increase in intensity at  $2,926\text{ cm}^{-1}$  signifies the involvement of methylene C-H asymmetrical/symmetrical stretch in the reduction process. This proves that synthesized  $\text{TiO}_2$  NPs were synthesized with *E. prostrata* compounds involved in the biological reduction of  $\text{TiO}_2$  (40).

The synthesized NPs were characterized by AFM for detail size, morphology, and agglomeration. Characterization of the synthesized NPs using AFM offered a three-dimensional visualization. The uneven surface morphology was explained by the presence of both individual and agglomerated NPs. The strong crystalline nature was observed in the form of diagonal formations with ridges (Fig. 2A and B). Previous studies reported topographical images of irregularly shaped synthesized NPs that were in accordance with the present results (41). TEM images showed that the synthesized Ag NPs and  $\text{TiO}_2$  NPs obtained were spherical and quite polydisperse, and individual particles showed average sizes of  $12.82 \pm 2.50\text{ nm}$  and  $83.22 \pm 1.50\text{ nm}$ , respectively. The selected area electron diffraction (SAED) pattern of the Ag NPs, the ring-like diffraction pattern, indicates that the particles were crystalline. The diffraction rings were indexed on the basis of the face-centered cubic (FCC) structure of silver. Four rings arise due to reflections from lattice planes 111, 200, 220, and 311 of FCC silver. In the SAED pattern of the  $\text{TiO}_2$  NPs, six rings arise due to reflections from lattice planes 110, 101, 111, 21, 220, and 301 of FCC titanium. This is evident from the sharp Bragg's reflection observed in the XRD spectrum (Fig. 2C and D).

**GC-MS analysis.** The retention times (RT) and peak areas of the individual compounds identified by GC-MS analysis in the aqueous leaf extracts of *E. prostrata* are shown in Table 1. Four compounds were detected in the aqueous leaf extract, and the major chemical constituent was identified as 2,3-dihydrobenzofuran (peak area, 27.44%), which could have acted as a reducing and capping agent for the synthesis of Ag NPs and  $\text{TiO}_2$  NPs. The other constituents, such as 1,3-dihydroisobenzofuran (19.97%), 4-choloro-2,5-dimethoxybenzamine (21.80%), and methyl-3-(hydroxymethyl)bicyclo[3.2.1]oct-6-ene-1-carboxylate (5.53%), were identified.

**Analysis of cell viability.** The results showed that the synthesized Ag NPs were most active against promastigotes of *L. donovani*, compared to aqueous leaf extract of *E. prostrata*, the  $\text{AgNO}_3$  and  $\text{TiO}(\text{OH})_2$  solutions, and the synthesized  $\text{TiO}_2$  NPs. Significance levels were estimated by one-way ANOVA followed by Dunnett's multiple-comparison test, and the differences were found to be highly significant ( $P < 0.001$ ) for synthesized Ag NPs (Table 2). Decreased mobility of promastigotes treated with aqueous leaf extract of *E. prostrata*, synthesized Ag NPs, and  $\text{AgNO}_3$  solution were observed under light microscopy in the first 24 h of treatment. Pronounced morphological changes within the parasite, such as a change from round to oval shape, a decrease in size with dense cytoplasm, and enlarged nuclei, were also observed. Soon after 24 h, the morphology of the treated promastigotes was completely destroyed. The  $\text{IC}_{50}$ s were determined at 24 h of treatment with synthesized Ag NPs. The result showed an  $\text{IC}_{50}$  log value of  $1.17\ \mu\text{g/ml}$ , which is equivalent to  $14.94\ \mu\text{g/ml}$  in promastigotes (Fig. 3A), and in intracellular amastigotes it was  $0.58\ \mu\text{g/ml}$  (log value), which is equivalent to  $3.89\ \mu\text{g/ml}$  (Fig. 3B, panel a). The antileishmanial activity of synthesized Ag NPs was also checked against the J774A.1 cell line to determine whether the doses used for  $\text{IC}_{50}$  determination for intracellular amastigotes

were toxic to the cell itself; experiments revealed that the 50% cytotoxic dose ( $\text{CC}_{50}$ ) was far higher ( $115.5\ \mu\text{g/ml}$ ) than the  $\text{IC}_{50}$  ( $3.89\ \mu\text{g/ml}$ ) for intracellular amastigotes (Fig. 3B, panel b).

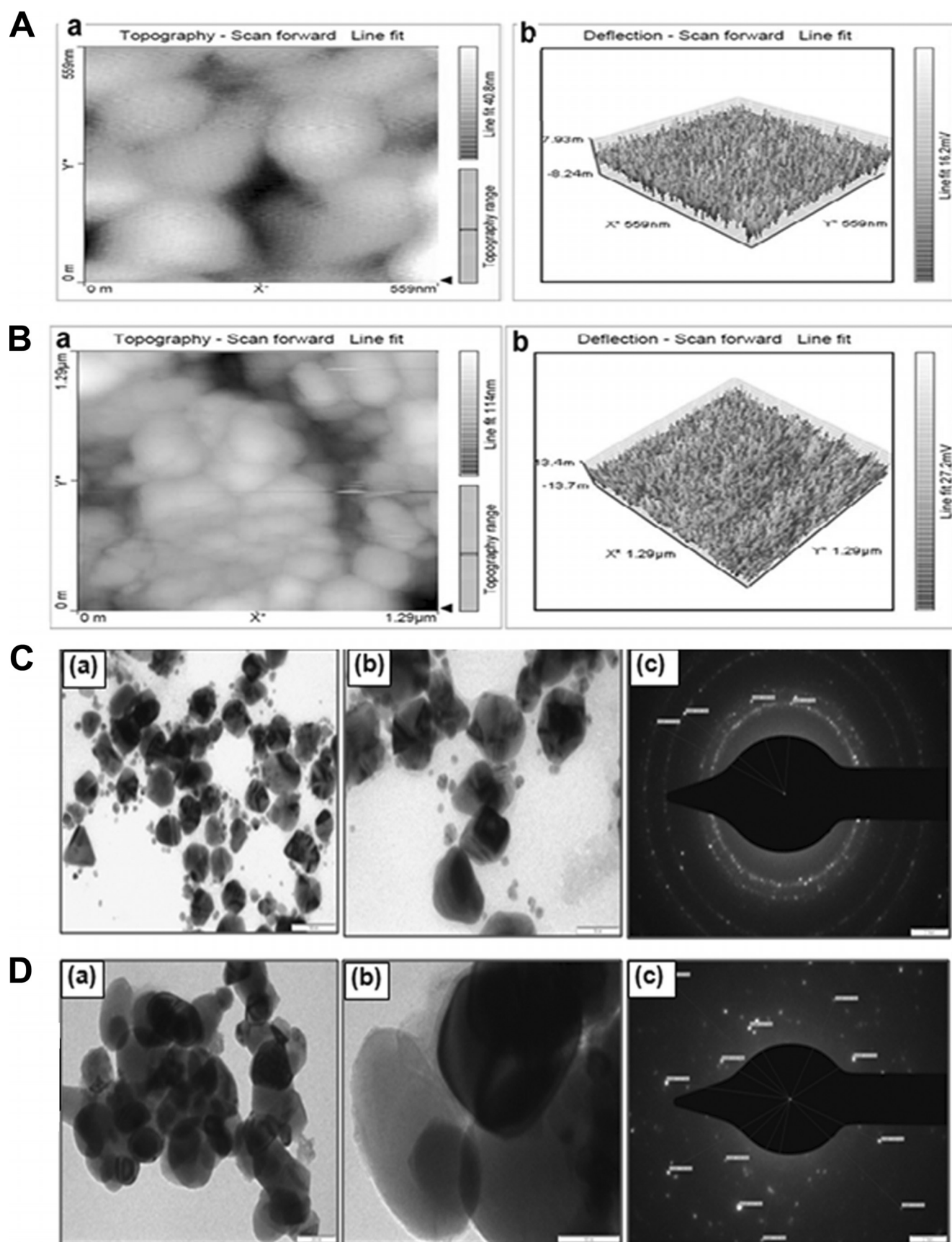
**Transmission electron microscopy.** TEM has been the most widely used technique to visualize agglomerated NPs in cells. The ultrastructural analysis of the promastigotes treated with synthesized Ag NPs showed cytolysis with features of necrosis, including a general cell hydration causing swelling of the organelles (endoplasmic reticulum and mitochondria), vacuolization, and gross alterations in the organization of the nuclear and chromatin compared to the controls (Fig. 3C).

**Propidium iodide uptake assay.** PI uptake was used to quantify the population of cells in which membrane integrity was lost, resulting in cell death. Different concentrations of synthesized Ag NPs were used to assess cellular uptake of PI in *L. donovani* promastigotes after 24 h treatment. This method has also been applied by other investigators (32, 33). Gould et al. (32) established that propidium-based cell lysis assay is a valuable and convenient new method for evaluating the interaction of drug candidates and target cells in culture. In Fig. 4A, the  $x$  axis depicts propidium iodide uptake and the  $y$  axis depicts side scatter (SSC). Gating of the PI-negative cells was done on the basis of their being unscattered, as depicted by the  $y$  axis SSC (M1). Hence, we show increased cell death on the  $x$  axis (M2) by the gradual shifting of the dead cell population (increased mean fluorescence intensity [MFI]) with an increased concentration of synthesized Ag NPs. Treated promastigotes undertake PI in a concentration-dependent manner. A sharp increase in PI-positive (M2) cells from 19.27 MFI at  $12.5\ \mu\text{g/ml}$  to 50.36 at  $25\ \mu\text{g/ml}$  and a gradual decrease thereafter to 48.01 at  $50\ \mu\text{g/ml}$  after 24 h of treatment. Untreated cells, which served as controls, showed no cell death.

**Analysis of externalized phosphatidylserine.** To delineate the nature of cell death, *L. donovani* promastigotes which had been treated with different concentrations ( $12.5$ ,  $25$ , and  $50\ \mu\text{g/ml}$ ) of synthesized Ag NPs for 24 h were harvested, washed with PBS, and double stained with annexin V-FITC and PI. The number of cells that were PI positive (upper left quadrant) gradually increased from 34.87, 39.90, and 44.01% at  $12.5$ ,  $25$ , and  $50\ \mu\text{g/ml}$ , respectively. These observations suggested that synthesized Ag NPs induced cell death by necrosis. The promastigotes treated with synthesized Ag NPs were positive for both annexin V and PI (upper right quadrant) and showed a decrease in apoptosis from 13.12 to 6.78% at  $12.5$  and  $50\ \mu\text{g/ml}$ , respectively (Fig. 4B). In contrast, only 0.18% of untreated cells, which served as controls, were annexin V and PI positive and showed cell death. These results are a confirmatory indication of shift from apoptosis to necrosis on treatment of *L. donovani* promastigotes with synthesized Ag NPs.

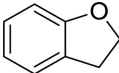
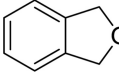
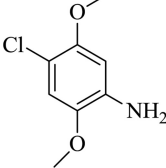
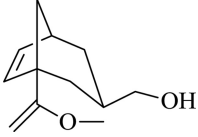
**Cell cycle analysis.** To assess the role of different concentrations ( $12.5$ ,  $25$ , and  $50\ \mu\text{g/ml}$ ) of synthesized Ag NPs in mediating  $G_0/G_1$  arrest and at the end of the treatment period (24 h), cell cycle analysis was performed based on PI staining using flow cytometry (42). Figure 4C shows that synthesized Ag NPs (at  $12.5$  and  $25\ \mu\text{g/ml}$ ) induced a marked increase in the number of cells in the  $G_0/G_1$  phase ( $G_1$ , 48.69% versus 60.50% to 62.00%), and simultaneous decreases in both S phase (S, 33.86% versus 31.73% to 27.70%) and  $G_2/M$  phase compared with the control were observed ( $G_2/M$ , 17.44% versus 7.76% to 10.30%). The concentration-dependent effect on  $G_0/G_1$  arrest in promastigotes was largely at the expense of S-phase cells, with low changes in the  $G_2/M$ -phase cell population compared with the untreated pro-





**FIG 2** (A) Atomic micrograph of synthesized Ag NPs with aerial (a) and three-dimensional (3D) (b) topographical views of the topological structures. (B) Atomic micrograph of synthesized TiO<sub>2</sub> NPs with aerial (a) and 3D (b) topographical views of the topological structures. (C) Transmission electron microscopy (TEM) micrograph showing size, shape, and morphology of synthesized Ag NPs (a and b) and SAED (selected area electron diffraction) (c). (D) TEM images of the synthesized TiO<sub>2</sub> NPs (a and b) and SAED (c).

TABLE 1 Chemical composition of the *E. prostrata* leaf extract identified by GC-MS<sup>a</sup>

RT	Identified molecule	Chemical structure	MF	MW	Peak area (%)
3.3	2,3-Dihydrobenzofuran		C <sub>8</sub> H <sub>8</sub> O	120	27.44
4.3	1,3-Dihydroisobenzofuran		C <sub>8</sub> H <sub>8</sub> O	120	19.97
18.5	4-Chloro-2,5-dimethoxybenzamine		C <sub>9</sub> H <sub>10</sub> ClNO <sub>2</sub>	187	21.80
22.6	Methyl-3-(hydromethyl)bicyclo[3.2.1]oct-6-ene-1-carboxylate		C <sub>10</sub> H <sub>14</sub> O <sub>3</sub>	182	5.53

<sup>a</sup> RT, retention time; MF, molecular formula; MW, molecular weight.

mastigotes. The drug-induced cell cycle perturbations, such as an increase in the number of cells in the G<sub>1</sub> phase, have been reported to correlate with a response to chemotherapy (43).

**DNA fragmentation assay.** Treatment of promastigotes with different concentrations (12.5, 25, and 50 μg/ml) of synthesized Ag NPs for 24 h revealed DNA breakage which was not extensive. High-molecular-weight DNA fragments of ~700 bp were observed (Fig. 4C, panel f), which reconfirmed that mode of cell death in promastigotes may be largely due to necrosis.

**TUNEL assays.** TUNEL assays were performed in order to verify whether the synthesized Ag NPs were able to induce DNA fragmentation in promastigotes of *L. donovani*. Propidium iodide (total cellular DNA) and fluorescein (apoptotic cells) were the two dyes used. Gating (R1) was done within the DNA area on the *y* axis (FL2-A) and the DNA width on the *x* axis (FL2-W), as shown in Fig. 5A.

In Fig. 5B, the *x* axis depicts DNA (propidium iodide, linear red

fluorescence, and FL2 channel), and the *y* axis depicts anti-BrdU-FITC (log green fluorescence and FL1 channel). Increasing concentrations of synthesized Ag NPs showed the increased number of cells (R2) stained by anti-BrdU which moved from the nonapoptotic population (G<sub>0</sub>/G<sub>1</sub> and G<sub>2</sub> phase) to the apoptotic population (S phase). We detected maximal DNA fragmentation in *Leishmania* cells exposed to 25 μg/ml of synthesized Ag NPs (Fig. 5B, panel e). These promastigotes showed an intense staining (9.78% TUNEL-positive cells) by anti-BrdU compared with untreated promastigotes (0.34% TUNEL-positive cells) (Fig. 5B, panel c).

Further detailed analysis of the S phase was done from the same data. By using the dual-parameter display method, not only were apoptotic cells resolved, but also, their stage in the cell cycle in terms of percentage of DNA content was determined. R1-gated cells (Fig. 6A) were divided into three subgates, which were R2, R3, and R4 (Fig. 6B). As shown in Fig. 6C, we further applied markers (M1, M2, and M3) on the subgates R2, R3, and R4 to denote G<sub>2</sub>, G<sub>3</sub>, and G<sub>4</sub>, depicting pre-S phase, S phase, and post-S phase, respectively. As can be seen by the histogram statistics (Fig. 6D), in comparison with the untreated cells, S-phase halt was prominent in cells treated with 25 μg/ml of synthesized Ag NPs (Fig. 6E). approximately 3-fold decrease in the percentage of DNA content in S phase of cells treated with synthesized Ag NPs was observed in comparison to untreated cells.

The length of S phase was further determined in terms of time of duration by following the protocol of Martynoga et al. (44). Gating was done using forward scatter (FSC) versus side scatter (SSC) (Fig. 7A). Fluorescence was measured in the log mode using CellQuest Pro software (BD Biosciences, CA), where the *x* axis depicts BrdU and the *y* axis depicts PI. Therefore, the ratio between the numbers of cells in the upper right (UR) quadrants and

TABLE 2 Analysis of cell viability test results by one-way ANOVA and Dunnett's multiple-comparison test<sup>a</sup>

Factor	% cell viability		<i>P</i>
	Mean	Standard deviation	
Ag NPs	0.255	0.015	<0.001
TiO <sub>2</sub> NPs	0.653	0.001	<0.001
Aqueous extract	0.359	0.007	<0.001
AgNO <sub>3</sub>	0.320	0.003	<0.01
TiO(OH) <sub>2</sub>	0.747	0.018	<0.001
Control	0.989	0.016	<0.001

<sup>a</sup> Significance between synthesized Ag NPs and aqueous leaf extract of *E. prostrata*, AgNO<sub>3</sub>, TiO(OH)<sub>2</sub> solution, and synthesized TiO<sub>2</sub> NPs. The lowest percent cell viability was found with synthesized Ag NPs. It was significantly lower than those obtained with all other factors.



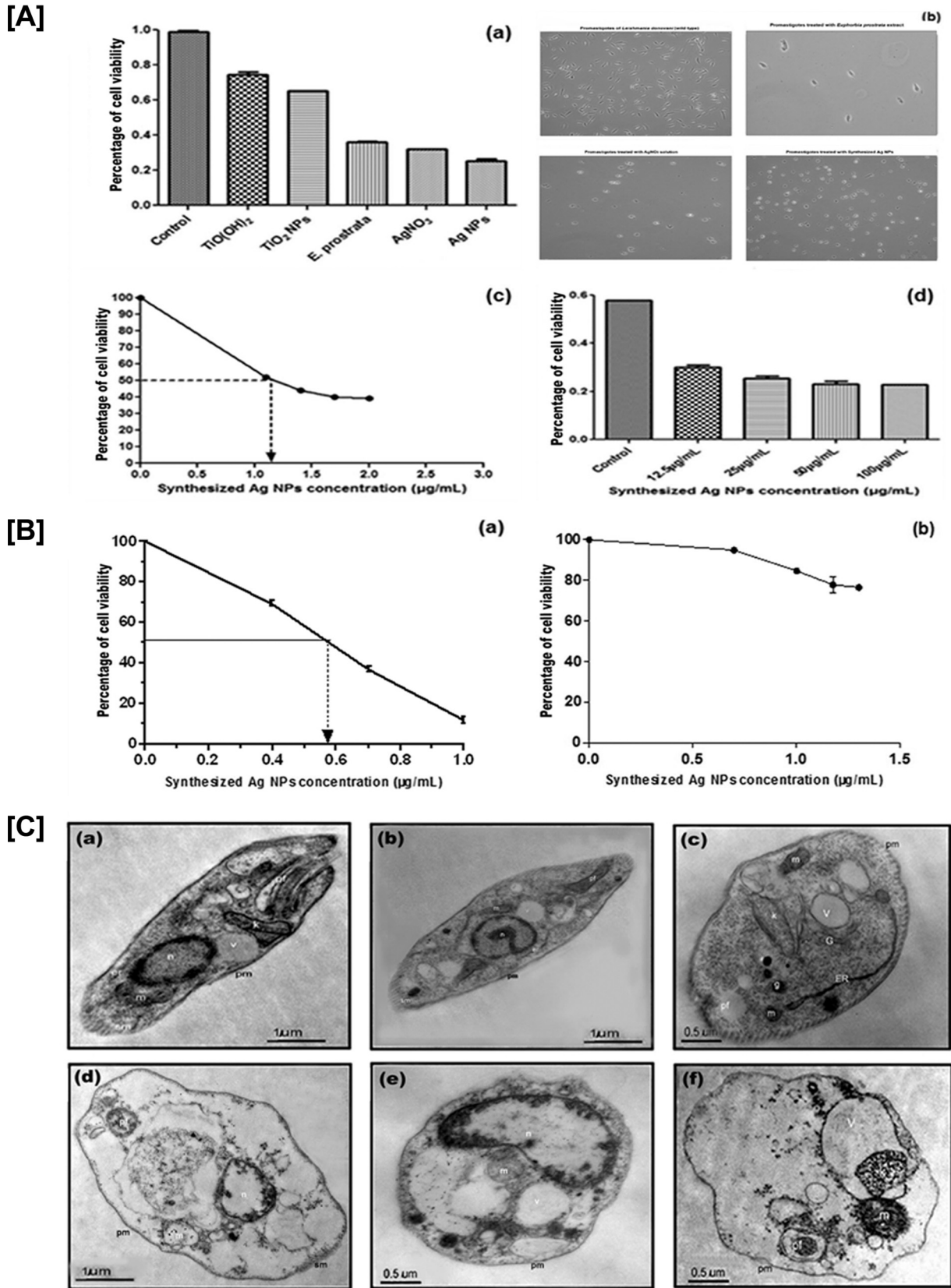


FIG 3 (A) Cell viability assessment by alamarBlue shows reduction in viability with different concentrations (0, 12.5, 25, 50, and 100 µg/ml) of synthesized-Ag NP-treated promastigotes. (a) Synthesized Ag NPs were most active against promastigotes of *L. donovani*, compared to aqueous extract of *E. prostrata* leaves, AgNO<sub>3</sub> solution, TiO(OH)<sub>2</sub>, synthesized TiO<sub>2</sub> NPs, and controls. (b) Microscopic images of wild-type promastigotes and promastigotes treated with aqueous

upper left (UL) quadrants is equal to the ratio of  $T_i$  (which equals 30 min) to  $T_s$ , when cells are exposed to PI and BrdU. We calculated the duration of S phase with the formula  $T_i/T_s = L \text{ cells/S cells}$  or  $T_s = T_i \times (\text{S cells/L cells})$ , where L (leaving) cells are BrdU<sup>-</sup> PI<sup>+</sup> cells (these cells in the initial BrdU-labeled S-phase cohort will leave S phase) and S cells are BrdU<sup>+</sup> PI<sup>+</sup> cells. Our calculations were based on histogram analysis (Fig. 7B and C), where BrdU<sup>-</sup> PI<sup>+</sup> cells were in the UL quadrant, and BrdU<sup>+</sup> PI<sup>+</sup> were in the UR quadrant. The UL quadrant showed ~1.47 and 1.16% PI<sup>+</sup> cells in untreated and treated cells, respectively, and the UR quadrant showed 2.01 and 4.35% BrdU<sup>+</sup> PI<sup>+</sup> cells in untreated and treated cells, respectively. Our results showed that the duration of S phase increased in parasites treated with synthesized Ag NPs (1.875 h) over that in untreated parasites (0.6836 h). The increased duration of S phase is responsible for the increased inhibition of proliferation of the cells in this phase. When S phase is lengthened (in terms of duration), the parasites become more dysregulated and exhibit reduced proliferation.

**Formation of ROS in *L. donovani*.** An inherent basic level of ROS production in wild-type promastigotes was detected, with a mean fluorescence intensity (MFI) of 82.66. Treatment of promastigotes with synthesized Ag NPs for 24 h revealed a gradual decrease of MFI in ROS generation from 34.35, 30.42, and 27.96 at 12.5, 25 and 50  $\mu\text{g/ml}$ , respectively, with respect to control cells (Fig. 8A). An established event in most apoptotic cells was the generation of ROS in the cytosol, which directs the cell and its neighboring cells toward the path of apoptotic cell death (45). Lower levels of ROS in our study could be a result of the antioxidant activity of the aqueous leaf extract of *E. prostrata*, which constituted the synthesized Ag NPs. Presumably this effect resulted in a shift from apoptosis to  $G_0/G_1$  arrest followed by necrotic cell death in *L. donovani*.

**Measurement of intracellular nonprotein thiols.** The fluorescent probe 5-chloromethyl fluorescein diacetate (CMFDA) was used to measure total intracellular nonprotein thiols after treatment of *L. donovani* promastigotes with aqueous leaf extract of *E. prostrata*, synthesized Ag NPs, and AgNO<sub>3</sub> solution. Synthesized Ag NPs showed a remarkable decrease in MFI (3.55) in comparison with that of the control cells (219.69) at 24 h. On analysis of our results, we found that the increase in MFI of intracellular nonprotein thiols (261.16) in comparison with that of the wild-type cells (219.69) was presumably a result of the antioxidant activity of the aqueous leaf extract of *E. prostrata*. Also, Ag was known to be an excellent effective trypanothione reductase (TR) inhibitor. In the present study, AgNO<sub>3</sub>-treated cells exhibited a remarkable decrease in MFI (5.67) in comparison with the wild-type cells (219.69) (Fig. 8B), thus lending credence to the above

statement. We infer that depletion of intracellular nonprotein thiols in *Leishmania* parasites treated with synthesized Ag NPs was independent of ROS generation. Our study therefore shows the important benefit of taking up these synthesized Ag NPs further for clinical development, as our green-synthesized NPs have the advantage of prevention of development of drug resistance. Overexpression of intracellular nonprotein thiols in *Leishmania* parasites is a known cause of drug efflux leading to resistance.

## DISCUSSION

Considering the efficacy of drugs available for the treatment of VL as well as their side effects and the resistance developed by parasites, the research in phytosciences, mainly regarding the properties of bioactive phytochemicals found in the crude extracts of medicinal plants, may lead to the discovery of new medicines with appropriate efficiency which are cheap and safe for patients. The concept of green NP synthesis was first developed by Raveendran et al. (46). Hence, the purpose of this research was to study the antileishmanial effects of synthesized NPs, including Ag and TiO<sub>2</sub>, on *L. donovani* parasites. The compound piceatannol isolated from the methanol extracts of another *Euphorbia* species, *Euphorbia lagascae*, was found to be moderately active against the promastigotes and more active against amastigotes of *L. donovani* (47). The green leaves of *E. prostrata* were selected for synthesis of NPs because they are the site of photosynthesis and availability of more H<sup>+</sup> ions to reduce the AgNO<sub>3</sub> and TiO(OH)<sub>2</sub> to Ag and TiO<sub>2</sub> NPs, respectively.

NPs synthesized either biologically or chemically must be characterized in order to understand their intrinsic properties, such as size, monodispersity, aqueous stability, net charge, adsorption to biomolecules, aggregation, and flocculation in various media (48). Our study provides vital information in this regard for both Ag and TiO<sub>2</sub> NPs. The reduction of ions and formation of stable NPs appeared quickly, within 6 h of reaction. Characterization via different microscopic techniques (TEM and AFM) and optical spectroscopy (UV-visible spectroscopy) proved to be very useful for the analysis of NPs. A distinct and fairly broad UV-Vis absorption band of Ag NPs was centered at 420 nm, which proved that the NPs were well dispersed without aggregation. The appearance of this band, which was assigned to a surface plasmon, is well documented for various metal NPs, with sizes ranging from 2 to 100 nm. Size distribution is a crucial parameter in determining the cellular uptake efficiency of the NPs and their transport through the cellular bilayer. The TEM analysis confirmed that the Ag NPs synthesized using *E. prostrata* were spherical, with an average size of  $12.82 \pm 2.50$  nm; *E. prostrata* leaf aqueous extract-synthesized TiO<sub>2</sub> NPs showed circular and irregular shapes and mostly aggre-

leaf extract of *E. prostrata*, AgNO<sub>3</sub> solution, and synthesized Ag NPs. Magnification,  $\times 60$ . (c) Percent cell viability plotted against log value of synthesized-Ag NP concentrations; IC<sub>50</sub>, 14.94  $\mu\text{g/ml}$ . (d) Percent cell viability of *L. donovani* promastigotes treated with synthesized Ag NPs. Data are means  $\pm$  standard deviations from three independent experiments. (B) (a) *In vitro* analysis of antileishmanial activity of synthesized Ag NPs in intracellular amastigotes (IC<sub>50</sub>). Macrophages (4,000 cells/well; final volume, 200  $\mu\text{l}$ ) were infected with promastigotes of *L. donovani* at a ratio of 6:1 (parasites/macrophages), and infected macrophages were treated with increasing concentrations (0, 2.5, 5, and 10  $\mu\text{g/ml}$ ) of synthesized Ag NPs for 24 h. After the indicated incubation times, treated and untreated cells were stained with Giemsa stain, and the slides were viewed on an inverted bright-field microscope (IX73 inverted microscope; Olympus). The IC<sub>50</sub> was obtained by plotting the graph of percentage of cell viability versus different concentrations of synthesized Ag NPs. The results are the means from duplicate experiments. (b) Cytotoxicity in macrophages (CC<sub>50</sub>). Macrophages (50,000 cells/well; final volume, 200  $\mu\text{l}$ ) were treated with increasing concentrations (0, 5, 10, and 20  $\mu\text{g/ml}$ ) of synthesized Ag NPs for 24 h. After indicated incubation time, the viability of the macrophages was estimated by MTT [3-(4,5-dimethylthiazole-2-yl)-2,5-diphenyl tetrazolium bromide] assay. The CC<sub>50</sub> was determined by logarithmic regression analysis using GraphPad Prism 5 software. Results are means  $\pm$  SD;  $n = 3$ . (C) Transmission electron microscopy of *L. donovani* promastigotes incubated with vehicle (a, b, and c) and synthesized Ag NPs (d, e, and f) at the IC<sub>50</sub> for 45 min. n, nucleus; k, kinetoplast; m, mitochondria; pf, pocket flagellar; pm, plasma membrane; G, Golgi body; g, glycosome; ER, endoplasmic reticulum.

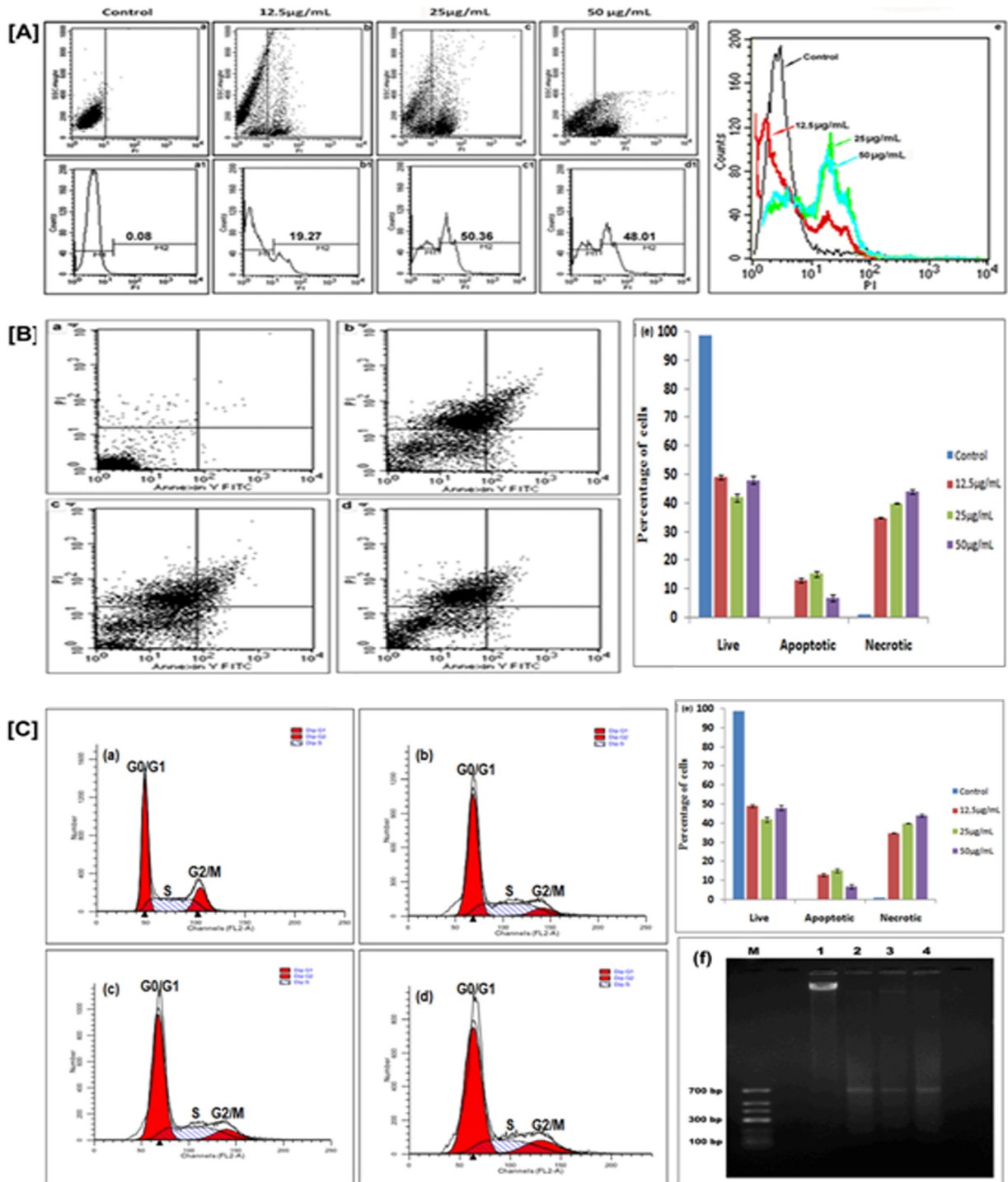


**FIG 4** (A) PI uptake analysis. Dot plots (a, b, c, and d) show that treatment of *Leishmania* parasites with synthesized Ag NPs leads to cell death (PI-positive cells, M2) (a1, b1, c1, and d1) in a concentration-dependent manner (e). (B) Externalization of phosphatidylserine in synthesized-Ag NP-treated promastigotes. *L. donovani* promastigotes were incubated with different concentrations of synthesized Ag NPs (0, 12.5, 25, and 50 µg/ml [a to d]) for 24 h and analyzed by flow cytometry. After the indicated incubation times, a significant number of membrane-compromised cells were stained positively by annexin V-FITC and PI (upper right quadrant) and by PI only (upper left quadrant). (e) Populations of live, apoptotic, and necrotic treated parasites. (C) Synthesized Ag NPs induced cell cycle arrest in the G<sub>0</sub>/G<sub>1</sub> phase of *L. donovani* parasites. After treatment with different concentrations of synthesized Ag NPs (0, 12.5, 25, and 50 µg/ml [a to d]) for 24 h, promastigotes were collected, washed with PBS, and stained with PI, and the DNA content was analyzed by flow cytometry. (e) Percentages of the population in G<sub>0</sub>/G<sub>1</sub>, S, and G<sub>2</sub>/M phase in treated parasites. (f) DNA fragmentation of *L. donovani* promastigotes treated with different concentrations of synthesized Ag NPs (12.5, 25, and 50 µg/ml). M, DNA ladder; lane 1, DNA from untreated cells; lanes 2, 3, and 4, DNA from synthesized-Ag NP-treated cells. Data are means ± standard deviations from three independent experiments.



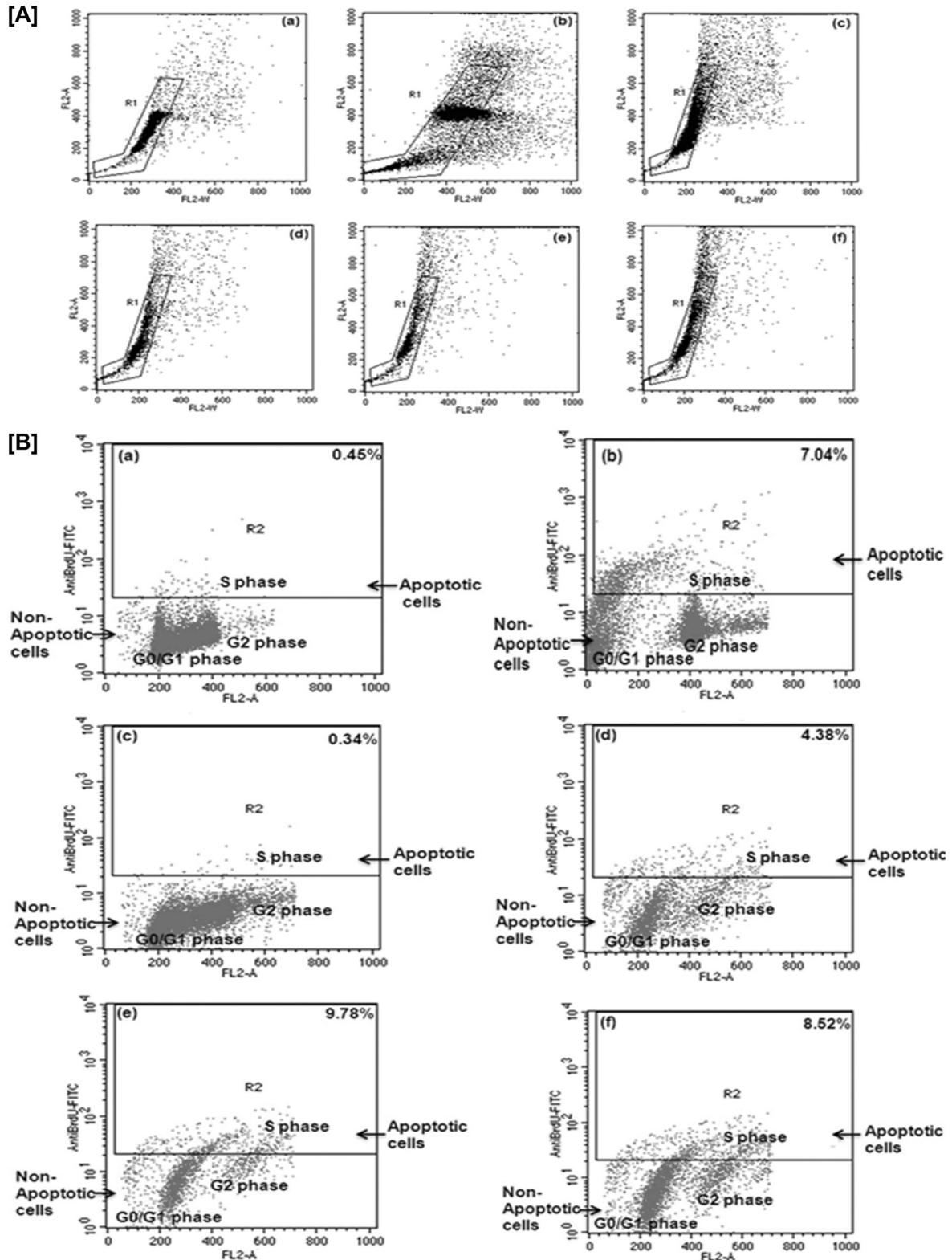
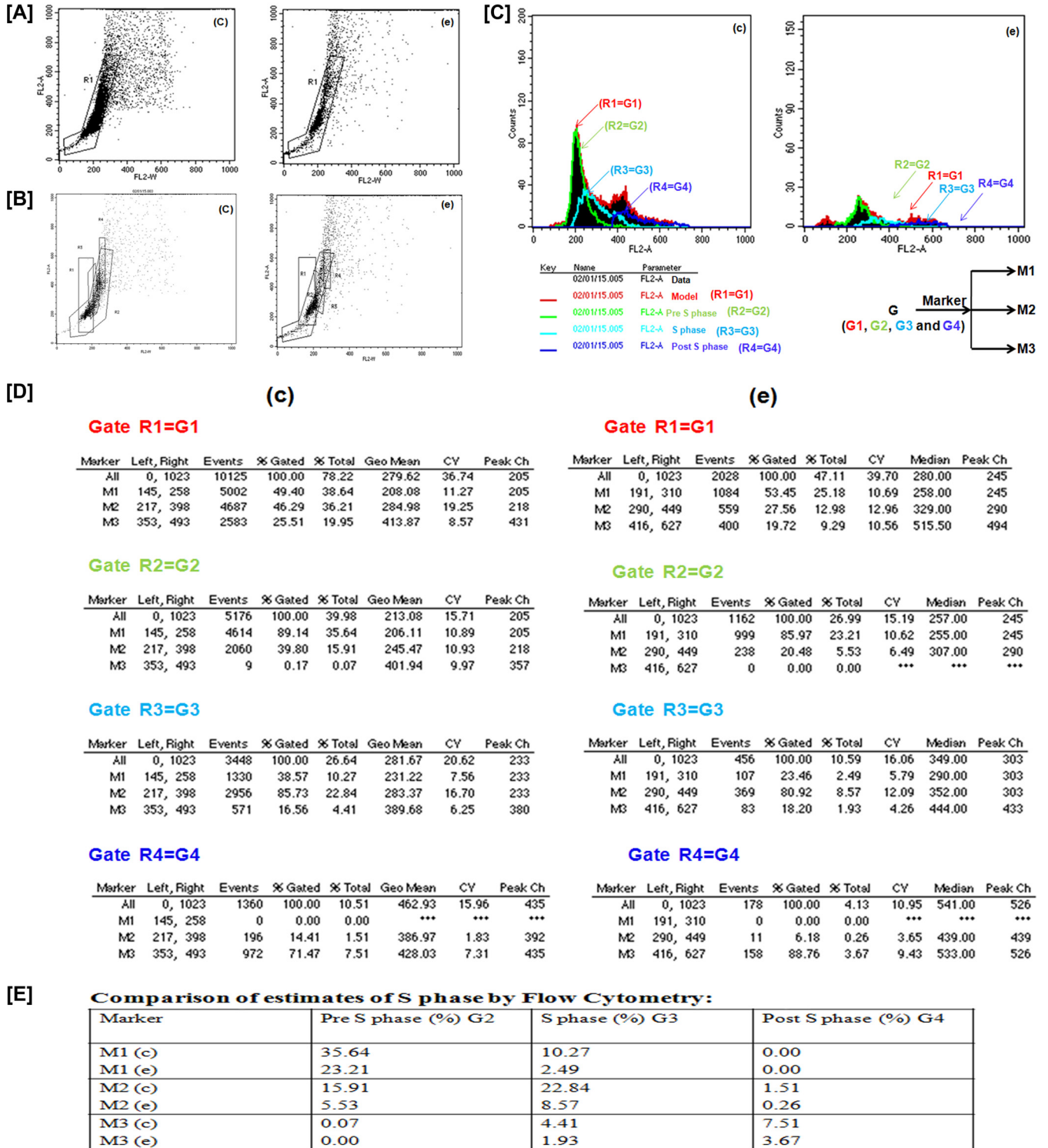
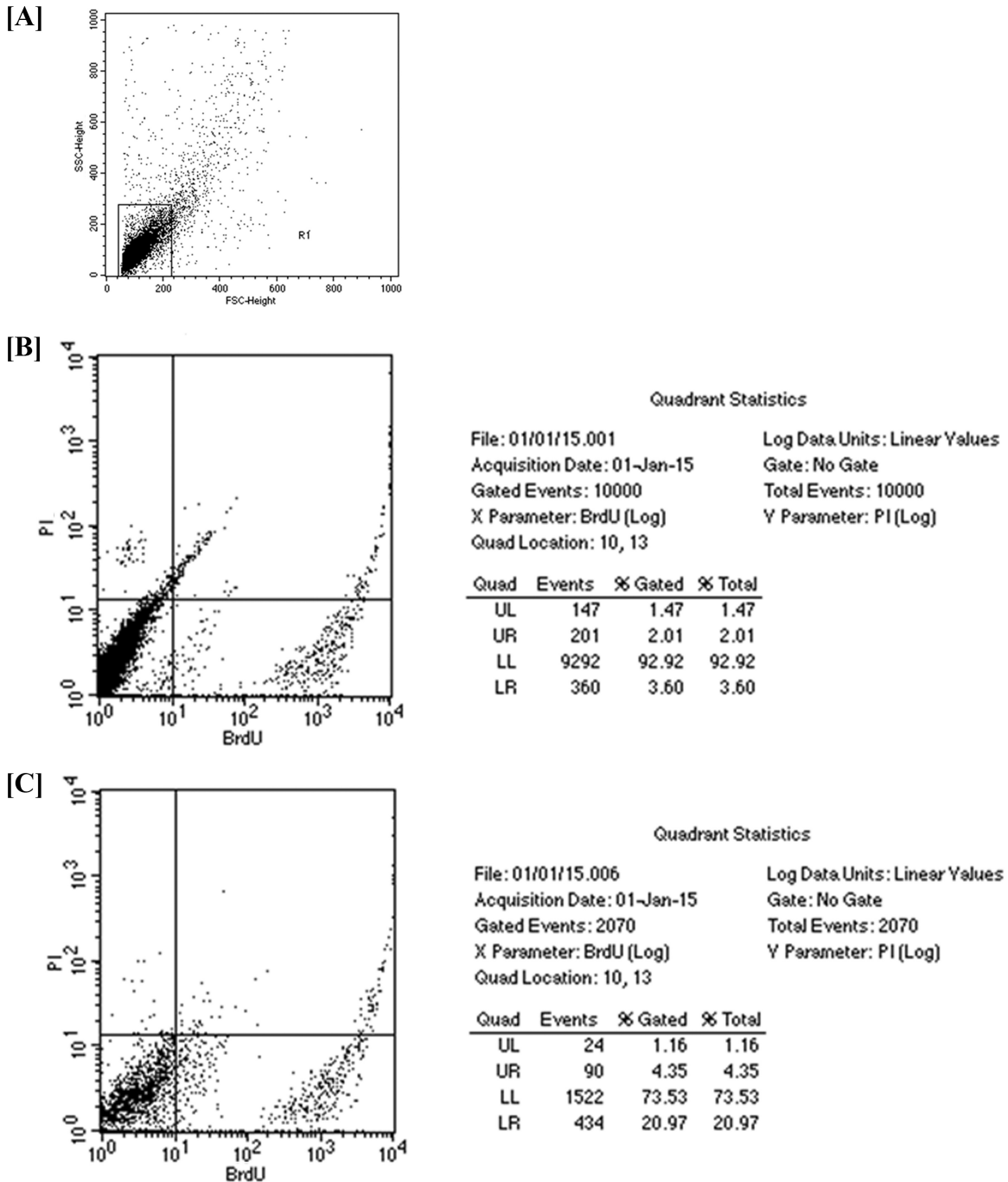


FIG 5 Synthesized-Ag NP-induced DNA fragmentation in promastigotes of *L. donovani* was analyzed by TUNEL assay using flow cytometry. (A) Gating was done with the DNA area on the y axis (FL2-A) and DNA width on the x axis (FL2-W). (B) A gate was drawn around the nonclumped cells. The x axis depicts DNA (FL2 channel) and the y axis depicts anti-BrdU-FITC (FL1 channel). Increasing concentrations of synthesized Ag NPs showed the increased number of cells (R2) stained by anti-BrdU, which have moved from a nonapoptotic population (G<sub>0</sub>/G<sub>1</sub> and G<sub>2</sub> phase) to an apoptotic population (S phase). (a and b) Negative and positive controls, respectively (provided with the kit); (c to f) promastigotes treated with different concentrations (0, 12.5, 25, and 50  $\mu$ g/ml, respectively) of synthesized Ag NPs.



**FIG 6** The length of S phase varies according to the percent DNA content in untreated and treated promastigotes of *L. donovani*. By using the dual-parameter display method, a gate was drawn around the nonclumped cells (R1) (A), and R1-gated cells were divided into three subgates, R2, R3, and R4 (B). (C) We further applied markers (M1, M2, and M3) to subgates R2, R3, and R4 to denote G<sub>2</sub>, G<sub>3</sub>, and G<sub>4</sub>, depicting pre-S phase, S phase, and post-S phase, respectively. (D) Statistical analysis of subgated cells of *L. donovani*. (E) S phase halt (in terms of percent DNA content) was prominent in cells treated with 25 μg/ml of synthesized Ag NPs, compared to untreated cells. In the “Marker” column, “c” and “e” indicate untreated parasites and parasites treated with 25 μg/ml of synthesized Ag NPs, respectively.



**FIG 7** The length of S phase, in terms of duration, was determined by the double-labeling method. (A) Gating was done using forward scatter (FSC) versus side scatter (SSC). (B and C) Fluorescence was measured in log mode using CellQuest Pro software (BD Biosciences, CA). (B) Histogram of untreated promastigotes; (C) histogram of promastigotes treated with 25 µg/ml of synthesized Ag NPs.

gated (and were thereby probably unable to be transported through the cellular bilayer of the parasite), with an average size of  $83.22 \pm 1.50$  nm.

It has been reported that individually, Ag NPs and the plant have antileishmanial properties. Our study shows an enhanced antileishmanial effect of the combination of the two. The antileishmanial activity of synthesized Ag NPs was significantly (four-fold) increased compared to wild-type parasites and was increased

approximately threefold when just the crude leaf extract or AgNO<sub>3</sub> solution was used to treat the parasites. The molecular mechanisms for this enhanced antileishmanial synergistic effect of combining AgNO<sub>3</sub> solution with aqueous leaf extract of *E. prostrata* were further confirmed by us to be multifactorial (Fig. 9).

Like Weingärtner et al. (49), who established that there is no phosphatidylserine in *Leishmania*, we too confirmed the absence of phosphatidylserine in the proteome of *L. donovani* DD8 (un-



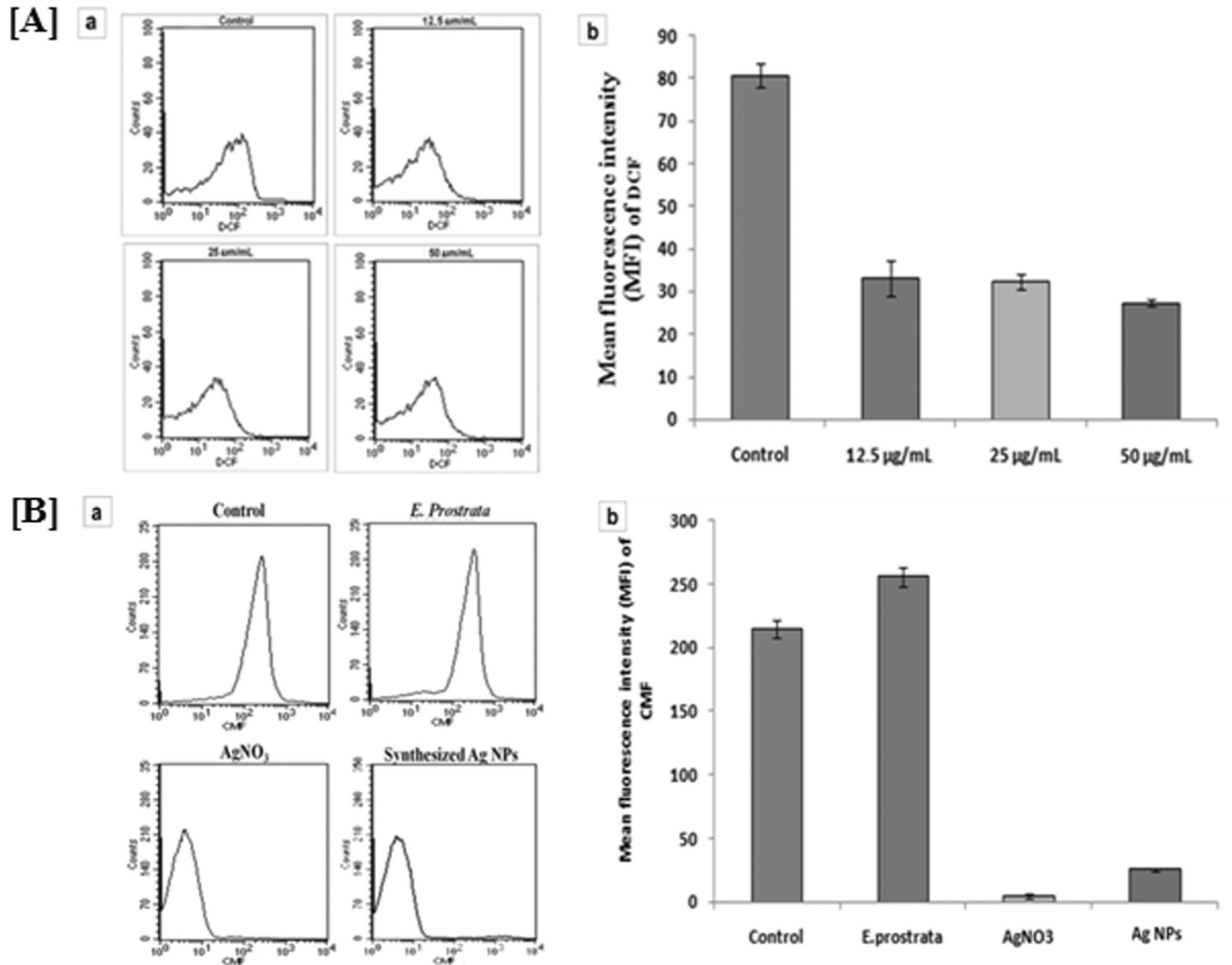


**FIG 8** (A) (a) ROS generation was measured using the fluorescent dye 2,7-dichlorodihydrofluorescein diacetate after treatment with different concentrations (12.5, 25, and 50 µg/ml) of synthesized Ag NPs for 24 h, and fluorescence was measured using a flow cytometer. (b) Mean fluorescence intensity of DCF in control and synthesized-Ag NP-treated cells at 24 h. Data are means ± standard deviations from three independent experiments. (B) (a) Intracellular level of the glutathione (GSH) in *L. donovani* promastigotes treated with *E. prostrata*, AgNO<sub>3</sub> solution, and synthesized Ag NPs. (b) Mean fluorescence intensity of CMF (GSH-sensitive probe) in control, *E. prostrata*-treated, AgNO<sub>3</sub>-treated, and synthesized-Ag NP-treated cells at 24 h. Data are means ± standard deviations from three independent experiments.

published results). However, other phospholipid classes which participate in apoptosis, like phosphatidylethanol sphingomyelin and phosphatidyl choline, can also enable annexin V staining, and therefore annexin V binding is used as an early indicator of apoptosis by many other investigators (35, 50). Our results of annexin V-FITC and PI indicated necrosis as shift from the UR to the UL quadrant of synthesized-Ag NP-treated parasites. Ultrastructural analysis was also indicative of necrosis. Initially, DNA fragmentation as detected by TUNEL indicated apoptosis. However, high-molecular-weight DNA fragmentation observed by gel electrophoresis is indicative of necrotic cell death (51).

Arrest of cell cycle in G<sub>0</sub>/G<sub>1</sub> phase led to S-phase halt and the inhibition of the proliferation of the parasites. We monitored S-phase progression in promastigotes treated with or without synthesized Ag NPs by flow cytometry following the method of Wheeler et al. (52), who reported that S phase can be monitored by

either cell cycle progression, microscope cytometry, flow cytometry, K/N configuration counts, or short-pulse BrdU. In synthesized-Ag NP-treated parasites, the length of S phase (pre-S, S, and post-S phase) appeared particularly short in terms of percent DNA content in comparison with untreated cells, leading to the inhibition of proliferation.

We found decreased ROS production in the synthesized-Ag NP-treated parasites, which is responsible for the caspase-independent necrotic cell death mechanism. Although nanoparticles have antimicrobial activity, however, silver and titanium dioxide nanoparticles are also known to induce oxidative stress *in vitro* and *in vivo* (53). In our study, the plant extract of *E. prostrata* and synthesized Ag NPs were found to possess maximum antioxidant activity. The main chemical constituent of *E. prostrata* extract is 2,3-dihydrobenzofuran, which is a known antioxidant (54). A high level of intracellular nonprotein thiol in *E. prostrata* plant

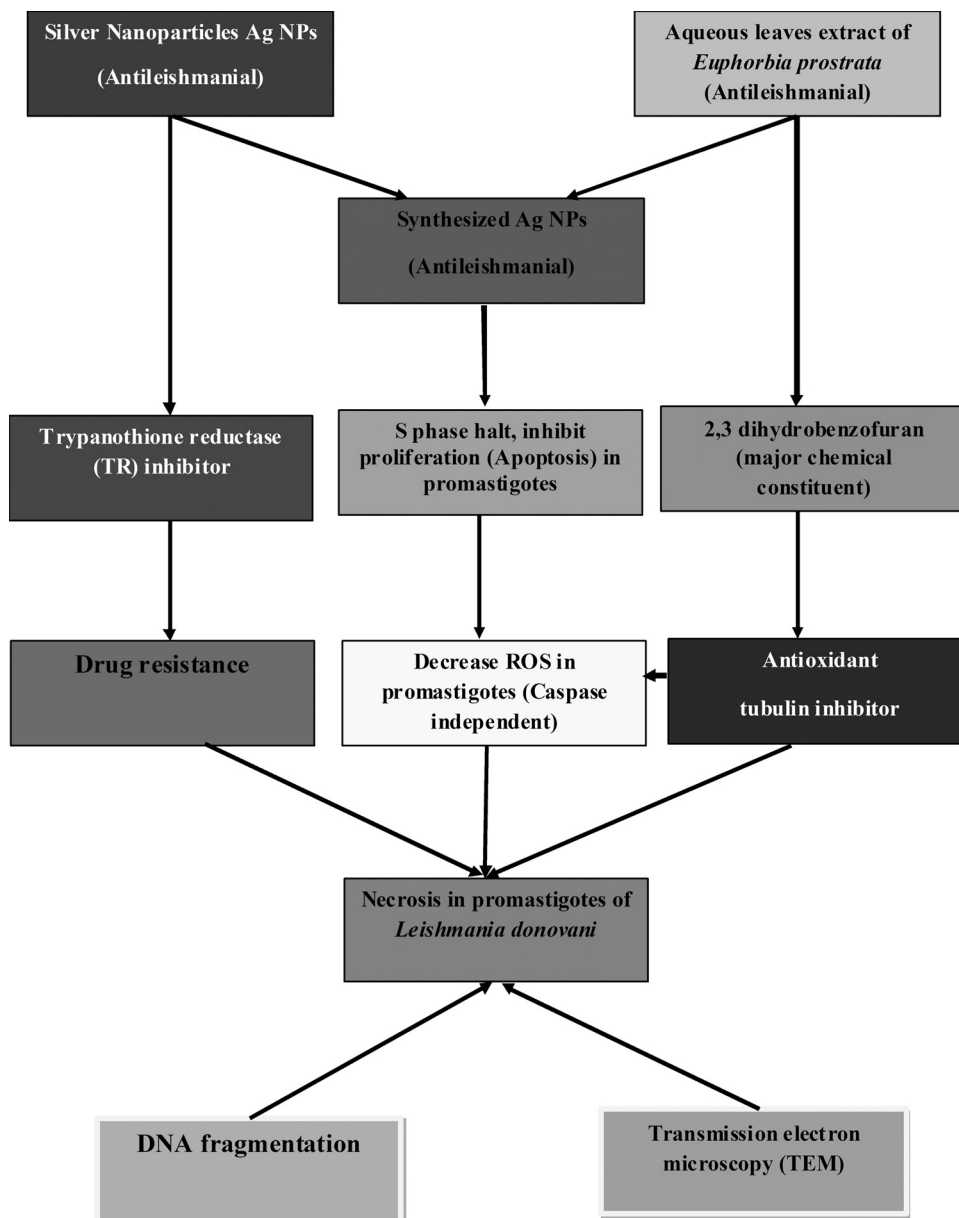


**FIG 9** Schematic diagram of proposed mechanism of synthesized-Ag NP-induced cell death in *L. donovani* promastigotes. Synthesized Ag NPs inhibited promastigote proliferation and induced caspase-independent cell death, which is largely due to necrosis. Cell death in *L. donovani* promastigotes is accompanied by decreased levels of intracellular nonprotein thiols and reactive oxygen species.

extract-treated parasites, compared to almost negligible levels in  $\text{AgNO}_3^-$  and synthesized-Ag NP-treated parasites, could be responsible for the quenching of ROS, because the low thiol levels within the cells treated with synthesized Ag NPs do not lead to adduct formation of efflux.

In *L. donovani*, the glutathione/glutathione reductase eukaryotic redox system is replaced by the unique trypanothione/trypanothione reductase (TR) system. Ag NPs are known to be an excellent effective TR inhibitor (55). This was corroborated by our results, which showed maximum TR inhibition in synthesized-Ag NP-treated promastigotes in comparison to promastigotes treated with aqueous leaf extract of *E. prostrata*. This can have an important implication for the treatment of clinical drug resistance with

synthesized Ag NPs. It has been established that 2,3-dihydrobenzofuran, the main chemical constituent of extract of *E. prostrata*, is also a promising antileishmanial lead molecule and contains antitubulin properties (56). This drug target of the parasite has a primary amino acid sequence different from that of its host. In conclusion, we can affirm from our studies that the synthesized Ag NPs could have a dual mode of leishmanicidal activity by targeting tubulins (dihydrobenzofuran of aqueous leaf extract of *E. prostrata*) or TR (Ag NPs).

#### ACKNOWLEDGMENTS

We are grateful to C. Abdul Hakeem (College Management), K. Masood Ahmed (Principal), and Hameed Abdul Razack (Head of Zoology Depart-

ment) for providing the facilities to carry out this work. The technical assistance of A.L. Vishwakarma regarding flow cytometry is acknowledged.

This work was supported by the Council of Scientific and Industrial Research (CSIR)-funded network project “Host Interactome analysis: Understanding the Role of Host Molecules in Parasitic Infection (HOPE).”

We have no conflicts of interest to declare.

## REFERENCES

- Desjeux P. 2004. Leishmaniasis: current situation and new perspectives. *Comp Immunol Microbiol Infect Dis* 27:305–318. <http://dx.doi.org/10.1016/j.cimid.2004.03.004>.
- Richard JV, Werbovetz KA. 2010. New antileishmanial candidates and lead compounds. *Curr Opin Chem Biol* 14:447–455. <http://dx.doi.org/10.1016/j.cbpa.2010.03.023>.
- Ezra N, Ochoa MT, Craft N. 2010. Human immunodeficiency virus and leishmaniasis. *J Global Infect Dis* 2:248. <http://dx.doi.org/10.4103/0974-777X.68528>.
- Kim BY, Rutka JT, Chan WC. 2010. Nanomedicine. *N Engl J Med* 363:2434–2443. <http://dx.doi.org/10.1056/NEJMra0912273>.
- Irache JM, Esparza I, Gamazo C, Agüeros M, Espuelas S. 2011. Nanomedicine: novel approaches in human and veterinary therapeutics. *Vet Parasitol* 180:47–71. <http://dx.doi.org/10.1016/j.vetpar.2011.05.028>.
- Morones JR, Elechiguerra JL, Camacho A, Holt K, Kouri JB, Ramírez JT, Yacamán MJ. 2005. The bactericidal effect of silver nanoparticles. *Nanotechnology* 16:2346. <http://dx.doi.org/10.1088/0957-4484/16/10/059>.
- Sinha S, Pan I, Chanda P, Sen SK. 2009. Nanoparticles fabrication using ambient biological resources. *J Appl Biosci* 19:1113–1130.
- Bhainsa KC, D'souza S. 2006. Extracellular biosynthesis of silver nanoparticles using the fungus *Aspergillus fumigatus*. *Colloids Surf B Biointerfaces* 47:160–164. <http://dx.doi.org/10.1016/j.colsurfb.2005.11.026>.
- Mohebbi M, Rezayat M, Gilani K, Sarkar S, Akhond B, Esmaeili J, Satvat T, Elikae S, Charehdar S, Hooshyar H. 2009. Nanosilver in the treatment of localized cutaneous leishmaniasis caused by *Leishmania major* (MRHO/IR/75/ER): an *in vitro* and *in vivo* study. *DARU J Pharm Sci* 17:285–289.
- Zampa MF, Araujo I, Costa V, Nery Costa CH, Santos JR, Jr, Zucolotto V, Eiras C, Leite JRS. 2009. Leishmanicidal activity and immobilization of dermaseptin 01 antimicrobial peptides in ultrathin films for nanomedicine applications. *Nanomedicine* 5:352–358. <http://dx.doi.org/10.1016/j.nano.2008.11.001>.
- Allahverdiyev AM, Abamor ES, Bagirova M, Ustundag CB, Kaya C, Kaya F, Rafailovich M. 2011. Antileishmanial effect of silver nanoparticles and their enhanced antiparasitic activity under ultraviolet light. *Int J Nanomed* 6:2705.
- Torabi N, Mohebbi M, Shahverdi AR, Rezayat SM, Edrissian GH, Esmaeili J, Charehdar S. 2011. Nanogold for the treatment of zoonotic cutaneous leishmaniasis caused by *Leishmania major* (MRHO/IR/75/ER): an animal trial with methanol extract of *Eucalyptus camaldulensis*. *J Pharm Health Sci* 1:13–16.
- Navarro L, Dunoyer P, Jay F, Arnold B, Dharmasiri N, Estelle M, Voinnet O, Jones JD. 2006. A plant miRNA contributes to antibacterial resistance by repressing auxin signaling. *Science* 312:436–439. <http://dx.doi.org/10.1126/science.1126088>.
- Wiesenthal A, Hunter L, Wang S, Wickliffe J, Wilkerson M. 2011. Nanoparticles: small and mighty. *Int J Dermatol* 50:247–254. <http://dx.doi.org/10.1111/j.1365-4632.2010.04815.x>.
- Das S, Roy P, Mondal S, Bera T, Mukherjee A. 2013. One pot synthesis of gold nanoparticles and application in chemotherapy of wild and resistant type visceral leishmaniasis. *Colloids Surf B Biointerfaces* 107:27–34. <http://dx.doi.org/10.1016/j.colsurfb.2013.01.061>.
- Sundrarajan M, Gowri S. 2011. Green synthesis of titanium dioxide nanoparticles by *Nyctanthes arbor-tristis* leaf extract. *Chalcogenide Lett* 8:447–451.
- Schmelzer GH, Gurib-Fakim A. 2008. Medicinal plants 1. PROTA Foundation. Backhuys Publishers, Wageningen, Netherlands.
- Rene K, Hortense GK, Pascal W, Jean Alexis M, Vidal PE, Michel Archange F, Christine FM. 2007. Activity of aqueous ethanol extract of *Euphorbia prostrata* ait on *Shigella dysenteriae* type 1-induced diarrhea in rats. *Indian J Pharmacol* 39:240. <http://dx.doi.org/10.4103/0253-7613.37275>.
- Kerboeuf D, Riou M, Guégnard F. 2008. Flavonoids and related compounds in parasitic disease control. *Mini Rev Med Chem* 8:116–128. <http://dx.doi.org/10.2174/138955708783498168>.
- Radtke OA, Foo LY, Lu Y, Kiderlen AF, Kolodziej H. 2003. Evaluation of sage phenolics for their antileishmanial activity and modulatory effects on interleukin-6, interferon and tumour necrosis factor-alpha-release in RAW 264.7 cells. *Zeitschrift Naturforsch C* 58:395–400.
- Sharma U, Singh D, Kumar P, Dobhal M, Singh S. 2011. Antiparasitic activity of plumericin & isoplumericin isolated from *Plumeria bicolor* against *Leishmania donovani*. *Indian J Med Res* 134:709. <http://dx.doi.org/10.4103/0971-5916.91005>.
- Parashar V, Parashar R, Sharma B, Pandey AC. 2009. *Parthenium* leaf extract mediated synthesis of silver nanoparticles: a novel approach towards weed utilization. *Digest J Nanomaterials Biostructures* 4:45–50.
- Veerasingh R, Xin TZ, Gunasagaran S, Xiang TFW, Yang EFC, Jeyakumar N, Dhanaraj SA. 2011. Biosynthesis of silver nanoparticles using mangosteen leaf extract and evaluation of their antimicrobial activities. *J Saudi Chemical Soc* 15:113–120. <http://dx.doi.org/10.1016/j.jscs.2010.06.004>.
- Horcas I, Fernandez R, Gomez-Rodriguez J, Colchero J, Gómez-Herrero J, Baro A. 2007. WSXM: a software for scanning probe microscopy and a tool for nanotechnology. *Rev Sci Instruments* 78:013705. <http://dx.doi.org/10.1063/1.2432410>.
- Ausloos P, Clifton C, Lias S, Mikaya A, Stein S, Tchekhovskoi D, Sparkman O, Zaikin V, Zhu D. 1999. The critical evaluation of a comprehensive mass spectral library. *J Am Soc Mass Spectrom* 10:287–299. [http://dx.doi.org/10.1016/S1044-0305\(98\)00159-7](http://dx.doi.org/10.1016/S1044-0305(98)00159-7).
- Kaur J, Kumar P, Tyagi S, Pathak R, Batra S, Singh P, Singh N. 2011. In silico screening, structure-activity relationship, and biologic evaluation of selective pteridine reductase inhibitors targeting visceral leishmaniasis. *Antimicrob Agents Chemother* 55:659–666. <http://dx.doi.org/10.1128/AAC.00436-10>.
- Kaur J, Sundar S, Singh N. 2010. Molecular docking, structure-activity relationship and biological evaluation of the anticancer drug monastrol as a pteridine reductase inhibitor in a clinical isolate of *Leishmania donovani*. *J Antimicrob Chemother* 65:1742–1748. <http://dx.doi.org/10.1093/jac/dkq189>.
- Ghosh S, Debnath S, Hazra S, Hartung A, Thomale K, Schultheis M, Kapkova P, Schurigt U, Moll H, Holzgrabe U. 2011. *Valeriana wallichii* root extracts and fractions with activity against *Leishmania* spp. *Parasitol Res* 108:861–871. <http://dx.doi.org/10.1007/s00436-010-2127-0>.
- Wong IL, Chan K-F, Chen Y-F, Lun Z-R, Chan TH, Chow LM. 2014. *In vitro* and *in vivo* efficacy of novel flavonoid dimers against cutaneous leishmaniasis. *Antimicrob Agents Chemother* 58:3379–3388. <http://dx.doi.org/10.1128/AAC.02425-13>.
- Chouhan G, Islamuddin M, Ahmad F, Sahal D, Afrin F. 2014. Antileishmanial Potential of *Piper nigrum* Seed Extracts against *Leishmania donovani*. *Open J Med Microbiol* 4:228. <http://dx.doi.org/10.4236/ojmm.2014.44025>.
- Rosa MDSS, Mendonça-Filho RR, Bizzo HR, de Almeida Rodrigues I, Soares RMA, Souto-Pradón T, Alviano CS, Lopes AHC. 2003. Antileishmanial activity of a linalool-rich essential oil from *Croton cajucara*. *Antimicrob Agents Chemother* 47:1895–1901. <http://dx.doi.org/10.1128/AAC.47.6.1895-1901.2003>.
- Gould MK, Vu XL, Seebeck T, de Koning HP. 2008. Propidium iodide-based methods for monitoring drug action in the kinetoplastidae: comparison with the Alamar Blue assay. *Anal Biochem* 382:87–93. <http://dx.doi.org/10.1016/j.ab.2008.07.036>.
- Gaur U, Showalter M, Hickerson S, Dalvi R, Turco SJ, Wilson ME, Beverley SM. 2009. *Leishmania donovani* lacking the Golgi GDP-Man transporter LPG2 exhibit attenuated virulence in mammalian hosts. *Exp Parasitol* 122:182–191. <http://dx.doi.org/10.1016/j.exppara.2009.03.014>.
- Kaur J, Singh BK, Tripathi RP, Singh P, Singh N. 2009. *Leishmania donovani*: a glycosyl dihydropyridine analogue induces apoptosis like cell death via targeting pteridine reductase 1 in promastigotes. *Exp Parasitol* 123:258–264. <http://dx.doi.org/10.1016/j.exppara.2009.07.009>.
- Marinho FA, Gonçalves KC, Oliveira SS, Gonçalves DS, Matteoli FP, Seabra SH, Oliveira ACS, Bellio M, Oliveira SS, Souto-Pradón T. 2014. The calpain inhibitor MDL28170 induces the expression of apoptotic markers in *Leishmania amazonensis* promastigotes. *PLoS One* 9:e87659. <http://dx.doi.org/10.1371/journal.pone.0087659>.
- Mukherjee SB, Das M, Sudhandiran G, Shaha C. 2002. Increase in cytosolic Ca<sup>2+</sup> levels through the activation of non-selective cation chan-



- nels induced by oxidative stress causes mitochondrial depolarization leading to apoptosis-like death in *Leishmania donovani* promastigotes. *J Biol Chem* 277:24717–24727. <http://dx.doi.org/10.1074/jbc.M201961200>.
37. Sarkar A, Mandal G, Singh N, Sundar S, Chatterjee M. 2009. Flow cytometric determination of intracellular non-protein thiols in *Leishmania* promastigotes using 5-chloromethyl fluorescein diacetate. *Exp Parasitol* 122:299–305. <http://dx.doi.org/10.1016/j.exppara.2009.04.012>.
  38. Dubey M, Bhadauria S, Kushwah B. 2009. Green synthesis of nanosilver particles from extract of *Eucalyptus hybrida* (safeda) leaf. *Dig J Nanomater Biostruct* 4:537–543.
  39. Liu Z, Hong L, Guo B. 2005. Physicochemical and electrochemical characterization of anatase titanium dioxide nanoparticles. *J Power Sources* 143:231–235. <http://dx.doi.org/10.1016/j.jpowsour.2004.11.056>.
  40. Coates J. 2000. Interpretation of infrared spectra, a practical approach, p 10815–10837. In R. A. Meyers (ed), *Encyclopedia of analytical chemistry*. John Wiley & Sons, Ltd., Chichester, United Kingdom.
  41. Logeswari P, Silambarasan S, Abraham J. 2012. Synthesis of silver nanoparticles using plants extract and analysis of their antimicrobial property. *J Saudi Chem Soc* 19:311–317.
  42. Kaur J, Dutta S, Chang K-P, Singh N. 2013. A member of the Ras oncogene family, RAPIA, mediates antileishmanial activity of monastrol. *J Antimicrob Chemother* 68:1071–1080. <http://dx.doi.org/10.1093/jac/dks507>.
  43. Efuert ET, Keyomarsi K. 2006. Farnesyl and geranylgeranyl transferase inhibitors induce G<sub>1</sub> arrest by targeting the proteasome. *Cancer Res* 66:1040–1051. <http://dx.doi.org/10.1158/0008-5472.CAN-05-3416>.
  44. Martynoga B, Morrison H, Price DJ, Mason JO. 2005. Foxg1 is required for specification of ventral telencephalon and region-specific regulation of dorsal telencephalic precursor proliferation and apoptosis. *Dev Biol* 283:113–127. <http://dx.doi.org/10.1016/j.ydbio.2005.04.005>.
  45. Chipuk JE, Green DR. 2005. Do inducers of apoptosis trigger caspase-independent cell death? *Nature Rev Mol Cell Biol* 6:268–275. <http://dx.doi.org/10.1038/nrm1573>.
  46. Raveendran P, Fu J, Wallen SL. 2006. A simple and “green” method for the synthesis of Au, Ag, and Au-Ag alloy nanoparticles. *Green Chem* 8:34–38. <http://dx.doi.org/10.1039/B512540E>.
  47. Duarte N, Kayser O, Abreu P, Ferreira MJU. 2008. Antileishmanial activity of piceatannol isolated from *Euphorbia lagascae* seeds. *Phytotherapy Res* 22:455–457. <http://dx.doi.org/10.1002/ptr.2334>.
  48. McNeil SE. 2011. *Characterization of nanoparticles intended for drug delivery*. Springer, New York, NY.
  49. Weingärtner A, Kemmer G, Müller FD, Zampieri RA, dos Santos MG, Schiller J, Pomorski TG. 2012. *Leishmania* promastigotes lack phosphatidylserine but bind annexin V upon permeabilization or miltefosine treatment. *PLoS One* 7:e42070. <http://dx.doi.org/10.1371/journal.pone.0042070>.
  50. Chowdhury S, Mukherjee T, Chowdhury SR, Sengupta S, Mukhopadhyay S, Jaisankar P, Majumder HK. 2014. Disuccinyl betulin triggers metacaspase-dependent endonuclease G-mediated cell death in unicellular protozoan parasite *Leishmania donovani*. *Antimicrob Agents Chemother* 58:2186–2201. <http://dx.doi.org/10.1128/AAC.02193-13>.
  51. Bicknell GR, Cohen GM. 1995. Cleavage of DNA to large kilobase pair fragments occurs in some forms of necrosis as well as apoptosis. *Biochem Biophys Res Commun* 207:40–47. <http://dx.doi.org/10.1006/bbrc.1995.1150>.
  52. Wheeler RJ, Gluenz E, Gull K. 2011. The cell cycle of *Leishmania*: morphogenetic events and their implications for parasite biology. *Mol Microbiol* 79:647–662. <http://dx.doi.org/10.1111/j.1365-2958.2010.07479.x>.
  53. Ganapathi AP, Devaki R, Thuniki NR, Manna J, Tirumuru B, Gopu CR, Deepthi SB, Trivedi R, Rana RK, Hasan A. 2014. *In vitro* assessment of Ag and TiO<sub>2</sub> nanoparticles cytotoxicity. *Int J Res Med Sci* 2:1360–1367. <http://dx.doi.org/10.5455/2320-6012.ijrms20141122>.
  54. Chen C-H, Chen C-H, Shaw C-Y, Chen C-C, Tsai Y-C. 2002. 2,3,4-Trimethyl-5,7-dihydroxy-2,3-dihydrobenzofuran, a novel antioxidant, from *Penicillium citrinum* F5. *J Nat Prod* 65:740–741. <http://dx.doi.org/10.1021/np010605o>.
  55. Baiocco P, Ilari A, Ceci P, Orsini S, Gramiccia M, Di Muccio T, Colotti G. 2011. Inhibitory effect of silver nanoparticles on trypanothione reductase activity and *Leishmania infantum* proliferation. *ACS Med Chem Lett* 2:230–233. <http://dx.doi.org/10.1021/ml1002629>.
  56. Van Miert S, Dyck SV, Schmidt TJ, Brun R, Vlietinck A, Lemière G, Pieters L. 2005. Antileishmanial activity, cytotoxicity and QSAR analysis of synthetic dihydrobenzofuran lignans and related benzofurans. *Bioorg Med Chem* 13:661–669. <http://dx.doi.org/10.1016/j.bmc.2004.10.058>.